Quaternary Science Reviews 207 (2019) 80–100

Contents lists available at ScienceDirect

Quaternary Science Reviews

journal homepage: www.elsevier.com/locate/quascirev

A remarkable Late Saalian (MIS 6) loess (dust) accumulation in the Lower Danube at Harletz (Bulgaria)

Pierre Antoine [a, *], France Lagroix [b], Diana Jordanova [c], Neli Jordanova [c], Johanna Lomax [d], Markus Fuchs [d], Maxime Debret [e], Denis-Didier Rousseau [f, g], Christine Hatté [h], Caroline Gauthier [h], Olivier Moine [a], Samuel N. Taylor [b], Jessica L. Till [b, i], Sylvie Coutard [j, a]

[a] Laboratoire de Géographie Physique: Environnements Quaternaires et Actuels, CNRS-Univ. Paris 1-UPEC, 92195, Meudon, France
[b] Institut de Physique du Globe de Paris, Sorbonne Paris Cité, Univ Paris Diderot, UMR 7154 CNRS, 75005, Paris, France
[c] National Institute of Geophysics, Geodesy and Geography, Bulgarian Academy of Sciences, Acad. G. Bonchev Str., Block 3, 1113, Sofia, Bulgaria
[d] Department of Geography, Justus-Liebig-University Giessen, 35390, Giessen, Germany
[e] UFR Sciences et Techniques, Université de Rouen, 76821, Mont-Saint-Aignan, France
[f] Laboratoire de Météorologie Dynamique, UMR CNRS-ENS 8539, Institute Pierre Simon Laplace, IPSL, Paris Sciences & Lettres (PSL) Research University, 75231, Paris, France
[g] Lamont-Doherty Earth Observatory of Columbia University, Palisades, NY, 10964, USA
[h] Laboratoire des Sciences du Climat et de l'Environnement, CEA-CNRS-UVSQ, Université Paris-Saclay, 91198, Gif-sur-Yvette, France
[i] Institute of Earth Sciences, University of Iceland, 101 Reykjavik, Iceland
[j] INRAP Hauts-de-France, 32 Avenue de l'Etoile du Sud, 80440, Glisy, France

ARTICLE INFO

Article history:
Received 16 April 2018
Received in revised form
16 December 2018
Accepted 7 January 2019

Keywords:
Pleistocene
Europe
Danube
Saalian
High-resolution
Luminescence dating
Grain size
Magnetic susceptibility

ABSTRACT

While numerous high-resolution studies concerning Last Glacial aeolian sequences are available for Europe, the approach of the penultimate glacial in this geographical area is still poorly developed. In order to bridge this gap, this study focuses on the Bulgarian sequence of Harletz, along the Danube River, where extremely high sedimentation rates allow the depiction of high-resolution signals during MIS 6. At Harletz in NW Bulgaria on the western bank of the Ogosta River (tributary of the Danube) a 20 m thick loess-palaeosols section was cleaned and sampled for a multi-disciplinary study and detailed pedostratigraphic approach. High-resolution continuous bulk sampling (5 cm) was carried out to characterise sedimentary grain size, magnetic properties (including magnetic susceptibility and its frequency dependence), colour reflectance (1 cm), and organic carbon. Geochronological control is based on 16 samples collected for OSL and MET-pIRIR dating. Using a cyclo-stratigraphic approach of the sequence combined with dating constraints provided by both MET-pIRIR dates and the age of a tephra layer occurring at a depth of 12 m within the main loess unit, we can demonstrate that the Harletz section exhibits a 10 m thick Late Saalian (Marine Isotope Stage 6, MIS 6) loess accumulation unique in Europe. The lower part of the main loess unit is 4 m thick and overlies a basal brown soil complex allocated to MIS 7, which includes an exceptionally thick (4 m) and detailed succession of loess and four incipient soil horizons never described in European loess until now. The closest and best-dated high-resolution palaeoenvironmental archive suitable for comparison comes from Lake Ohrid located about 400 km to the SW of Harletz. The Ohrid palynological record shows a progressive step-by-step evolution in climate and in environmental change during the transition between MIS 7 and MIS 6 from which a parallel with the Harletz pedosedimentary succession can be proposed. During the younger part of MIS 6 (160-129ka), steppe vegetation with abundant herbs (*Artemisia*) is dominant in the Lake Ohrid record, in good accordance with a global enhancement of aeolian dynamics, especially well recorded in sections located close to the Danube River from Serbia to Bulgaria and Romania (L2 loess). According to interpretations stemming from this study, the silts and fine sands building the Harletz loess section would have been transported from the Danube braided river system located (at that time) at about 4.5 km to the NW. Based on our data, the main loess units are characterised by a very low to a total absence of coarse sand particles. By contrast, during the Eemian interglacial (MIS 5e), and to a lesser extent throughout MIS 5 and during MIS 3 interstadials, the long distance transport of silt and fine sand particles is stopped and a weak aeolian sedimentation is likely driven by north-easterly winds transporting coarse sand grains

* Corresponding author.
E-mail address: pierre.antoine@lgp.cnrs.fr (P. Antoine).

https://doi.org/10.1016/j.quascirev.2019.01.005

from the proximal Ogosta River sandy banks. Finally, the weak development of Last Glacial loess (4 m max.) likely results from a rapid infilling of the sedimentary trap during the Saalian, then followed by a strong anthropogenic erosion of the topsoil and of the upper part of the loess profile since the Early Holocene (Neolithic).

1. Introduction

The impact of rapid climatic events such as the Dansgaard-Oeschger (D-O) cycles on records of European environments during the Last Glacial has been the focus of many research studies over the last 20 years (Sánchez Goñi et al., 1999, 2002, 2008; Müller et al., 2003; Desprat et al., 2007; Seelos et al., 2009; Boch et al., 2011; Moreno et al., 2014; Heiri et al., 2014; Luetscher et al., 2015). Bringing valuable contributions to this collective effort are investigations of European loess sequences based on multi-proxy analyses, continuous high-resolution sampling and luminescence and ^{14}C dating (Antoine et al., 2001, 2009a; Haesaerts et al., 2003; Rousseau et al., 2007, 2011; Gocke et al., 2014; Újvári et al., 2014, Moine et al., 2017). Studies of loess sequences have provided evidence of the extreme sensitivity of European environments to millennial climatic cycles (D-O cycles) during the Last Glacial (Hatté et al., 1998; Antoine et al., 2001, 2009a,b, 2013, 2016; Moine et al., 2002, 2008; Rousseau et al., 2002, 2007, 2011, 2017a,b). Continued loess investigations searching to resolve the impact of D-O climate cycles systematically from north-western to central Europe now logically move towards the Lower Danube loess area (Fig. 1A), well known for its very thick loess sections as in Serbia (Titel Plateau: Marković et al., 2009, 2015; Varga et al., 2012; Surduk: Fuchs et al., 2007; Antoine et al., 2009b) or in the Czech Republic (Dolní Věstonice: Antoine et al., 2013, Rousseau et al., 2013; Zeměchy: Hošek et al., 2015, Dunaszekcső: Újvári et al., 2018).

The above-mentioned studies have predominantly focused on Last Glacial dust accumulation. Throughout Europe, investigations of Penultimate glacial loess sequences are sparse (Kukla, 1977; Marković et al., 2015; Hérisson et al., 2016) despite observations of

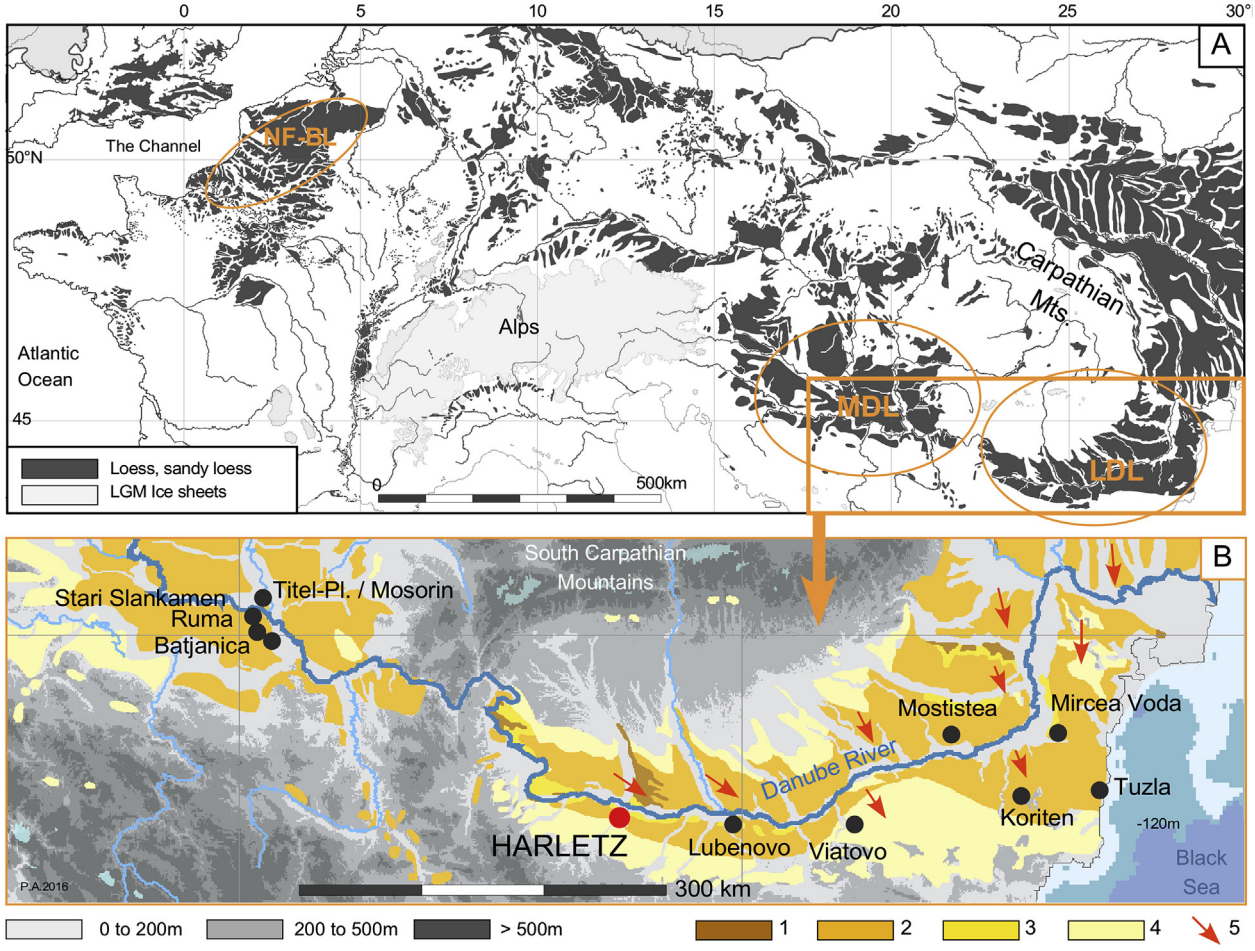

Fig. 1. Loess distribution in Europe. A) Location of the Lower (LDL) and Middle Danube (MDL) loess area and of Northern France and Belgium (NF-BL) loess area, in a simplified map of the European loess belt. B) Location of the Harletz and of other main regional loess-palaeosol sequences from Serbia to the Black Sea (loess map: according to Antoine et al., 2013, modified from Haase et al., 2007).
1) Aeolian sands, 2) Sandy loess, 3) Loess (>5 m), 4) Loess (<5 m), 5) Some palaeo-wind directions from the Lower Danube loess area according to Rozycki (1967).

rapid (millennial) climatic variations during marine isotope stage (MIS) 6 (ca. 170 and 140 ka) in marine sediment records (Martrat et al., 2004, 2007; Margari et al., 2010; Barker et al., 2011; Mokeddem and McManus, 2016), in lacustrine continental records (Sirocko et al., 2016; Sadori et al., 2016; Francke et al., 2016), and even in Chinese loess sequences (Yang and Ding, 2014). To bridge this gap, Bulgarian loess sequences are potentially ideal candidates. Located in the Lower Danube area, approximately 300 km downstream of the Titel Plateau in Serbia (Fig. 1B), important loess accumulations up to 40–60 m in thickness spanning the last 780 ka can be found (Jordanova et al., 2007; Jipa, 2014). Moreover, especially thick (>6 m) MIS 6 (or L2) loess unit is preserved in this area. Despite the great potential of Bulgarian loess, there are few documented studies (Jordanova and Petersen, 1999; Jordanova et al., 2008) and the sequences' chronologies are weakly constrained (Avramov et al., 2006). In 2012, a group of multi-disciplinary researchers in collaboration with the Bulgarian Academy of Science aimed to remedy the situation. Thick loess sequences spanning many hundreds of thousands of years covering the eastern parts of Bulgaria and Romania (Radan, 2012) were investigated. In northwestern Bulgaria, in the vicinity of the village of Harletz, loess thicknesses covering the T2 terrace are lesser, on the order of 20 m, but they also span a shorter time period based on magnetic susceptibility stratigraphic correlations (Avramov et al., 2006), thus resulting in higher resolution records.

The sequence of Harletz (43°41′52.78" N/23°49′42.27" E/altitude ca. 40 m a.s.l.) is located on the left bank of the Ogosta River, about 7 km to the southeast of its confluence with the Danube (Figs. 1B and 2). The studied section is a natural sub-vertical (ca. 70°) outcrop resulting from the erosion of the loess cover in the concavity of a meander of the Ogosta River, currently inactive. Owing to the very good preservation of the meander bars in the present-day alluvial plain, this erosion likely occurred during the Holocene (Fig. 2). The geology of the area has been investigated in detail (Evstatiev et al., 2000; Evlogiev, 2015) motivated by the Kozloduy Nuclear Power Plant, located 6 km to the east-northeast on the right bank of the Danube (Fig. 2). The Harletz loess sequence, thus, overlies an alluvial terrace body (sand and gravels) corresponding to the T2 level of Evlogiev (2015) (Fig. 3). The basal contact between these fluvial sediments and the bedrock (Pliocene silty clay) is located at about 25 m above sea level, at a similar altitude than the top of the current flood plain of the Danube, in a slightly stepped-terrace configuration whose morphology is largely hidden by a loess cover as thick as 40 m in the upper part of the slope (Fig. 3, Evstatiev et al., 2000). In the absence of accurate topographic data for the Ogosta River valley, we rely on *Google Earth* altitudes based on the 2015 copyrighted CNES image provided by the SPOT 5 satellite which has an in-plane accuracy of 10 m and a vertical accuracy of 5 m, comparable with conventional 1:50 000 scale mapping. The Ogosta River (surface: ca. 30 m a.s.l.) is currently weakly incised (ca. 2–3 m lower) with respect to the base of the Harletz loess-palaeosol sequence.

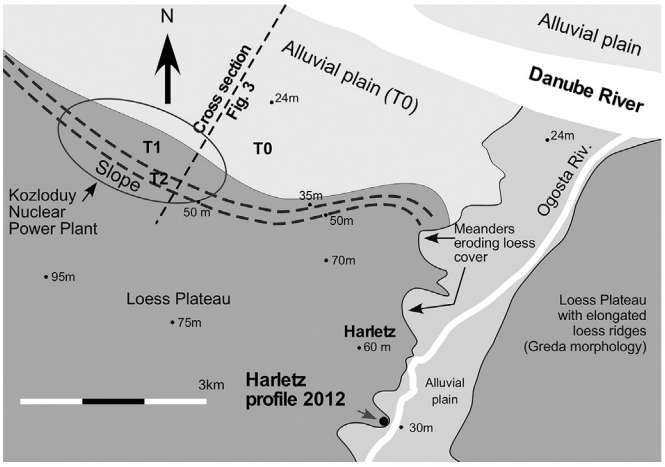

Fig. 2. Detailed location and geomorphology of the Kozloduy-Harletz area. Location of the Harletz-2012 (HZ12) section and of the cross-section of Fig. 3 (topography according to *Google Earth* Pro 2018; *Image © 2015 CNES/SPOT image*).

The area is presently characterised by a continental climate with mean annual temperature of 11 °C, mean January temperature of -2 °C, and mean July temperature of 23 °C (Fotakieva and Minkov, 1966). Mean annual precipitation ranges between 500 and 600 mm per year with a maximum in the summer months. Present topsoil is a typical Chernozem but since the Early Neolithic it has repeatedly been partially or totally eroded by human activity (Giosan et al., 2012).

The aim of this paper is to:

1) Present a detailed overview of the pedo-stratigraphy and sedimentology of the Harletz record including comparisons with magnetic susceptibility, TOC, $CaCO_3$ and colour reflectance data and luminescence dating and discuss both palaeoclimate and palaeoenvironmental implications.
2) Correlate the Harletz loess sequence with other European sequences as well as with other continental and marine palaeoclimate and palaeoenvironmental records that have geochronologically well-constrained palaeoclimate signals.

2. Material and methods

2.1. Field description and sampling

The vertical section was exposed by intensively removing the thick accumulation of reworked loess debris, which accumulated naturally on the steeply (ca. 70°) sloping concave meander wall carved by the Ogosta River. The section excavation resulted in 8 vertical panels of 2–3 m in height forming a series of steps carefully connected and metered using a hand-level (Fig. 4). The Harletz sequence totals 20 m in vertical depth and was continuously and accurately logged (scale of field drawing: 1/10). Colour is a fundamental parameter for the description of loess-palaeosol sequences, controlled by variations of the major mineral and organic components of soils and sediments: quartz, carbonates, iron and Fe-Mn oxides and oxyhydroxides and organic matter. Their relative variations are directly driven by climate and environmental conditions. The detailed and coloured log drawn from the Harletz section, shown in Fig. 5, follows an original approach developed (e.g. Haesaerts et al., 2003, 2016; Antoine et al., 2009a,b, 2013) to produce more realistic and useful logs of investigated sections than the traditionally published (over) simplified black (soil and palaeosol) and white (loess) sequence logs.

Bulk sampling for sedimentological, magnetic and geochemical analyses followed the continuous column sampling methodology (Antoine et al., 2009a) with a 5 cm depth-resolution. An extruding column with an approximate cross-section of 5 × 6 cm was sliced every 5 cm to produce homogenized bulk samples of about 300 g. This step was conducted with extreme caution avoiding and (or) systematically removing traces of biotubules that may pollute the analytical signal with their clayed-humic infillings originating from surface material. A total of 400 bulk samples were collected. In addition, a set of 10 undisturbed blocks where extracted from various soil horizons and sediments for thin section preparation and micromorphological observations. These along with other field observations are summarised in Table 1.

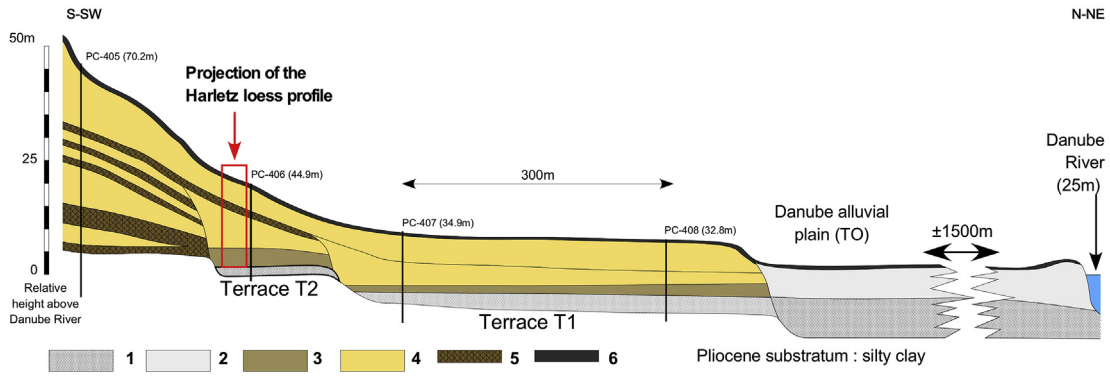

Fig. 3. Stratigraphical cross-section of the right bank of the Danube River valley highlighting fluvial terraces (T1 and T2) and loess cover. Location of the Harletz profile on the T2 terrace according to topographic and stratigraphic data (redrawn from Evlogiev, 2015).
1) Fluvial sands and gravels, 2) Fluvial silts and clays (T0), 3) Fluvial sandy silts (T1) and clayey sandy silts (T2), 4) Loess and sandy loess, 5) Palaeosol horizons, 5) Top soil (chernozem).

Fig. 4. General view of the Harletz section during preparation works, showing the succession of the vertical steps making the profile (photograph taken by M. Fuchs).

2.2. Sedimentological analyses

2.2.1. Grain size

Grain size analyses were performed with a Coulter LS-230 operating at the CNRS Meudon laboratory and followed the protocol developed for the study of European loess sequences (Antoine et al., 2009a). Ten grams of bulk sample was homogenized, dispersed in a solution of sodium hexameta-phosphate, and placed in a rotary shaker for 2 h. The sediment is sieved at 160 μm to remove coarse sand grains, calcareous concretions and other debris from calcified roots or mollusc shells, which may disturb the results of laser analysis. The mass of the larger than 160 μm fraction is reported as a percentage of the initial sample mass (10 g). Coulter LS-230 analyses are conducted on the less than 160 μm fraction and calibrated on a series of 17 test samples representative of the various facies following the standard Robinson sieving and pipette method (Soil Analysis Laboratory of INRA-Arras, Table 2). Such a calibration is particularly important with regards to clay content and determining the upper limit of clay grain size of laser data. For the Harletz sequence, the calibration results in clay sizes extending to 6 μm for the Coulter LS-230 data, in accordance with previous results on similar type of sediment (Konert and Vandenberghe, 1997; Antoine et al., 2013), whereas classically the upper clay grain size is set at 2 μm. Finally, two grain size ratios are calculated: Grain Size Index (GSI) of Antoine et al. (2009a) defined as the ratio between coarse silts (20–63 μm) and the sum of fine silts (6–20 μm) and clays (≤6 μm) and Coarse Silt Index (CSI) of Schirmer (2016) defined as the ratio between coarse silts (20–63 μm) and fine silts (6–20 μm).

2.2.2. Organic and carbonate content

The sediment samples (400) were dried out at low temperature as soon as possible to ensure safe storage, as recommended by Gauthier and Hatté (2008). After being sieved at 200 μm to remove coarse sand grains, $CaCO_3$ concretions (calcified root tracks) and mollusc shells, and being homogenized, the sediment then underwent a soft leaching process to remove carbonate using pre-combusted glass beakers, HCl 0.6N at room temperature, ultra-pure water and drying at 50 °C. The samples were then crushed in a pre-combusted glass mortar for homogenization prior to carbon and carbonate content evaluation. The handling and chemical procedures are common precautions employed with low-carbon-content sediments.

Two different carbon measurements were performed for every sediment sample: total carbon for the bulk sediments and organic carbon for the leached sediments. Approximately 15–20 mg of sediment was weighed in tin cups for measurement (with a precision of 1 μg). The sample was combusted in a ThermoFinigan Instrument Flash EA 1112 Elemental Analyser, and the carbon content determined using the Eager software.

A standard was inserted as unknown every 10 samples. The inorganic carbon content in the bulk sediment was calculated by assuming that mineral carbon exists only as $CaCO_3$. The results are reported in %weight of carbonate/bulk sediment and in %weight of organic carbon/bulk sediment and shown in Fig. 5.

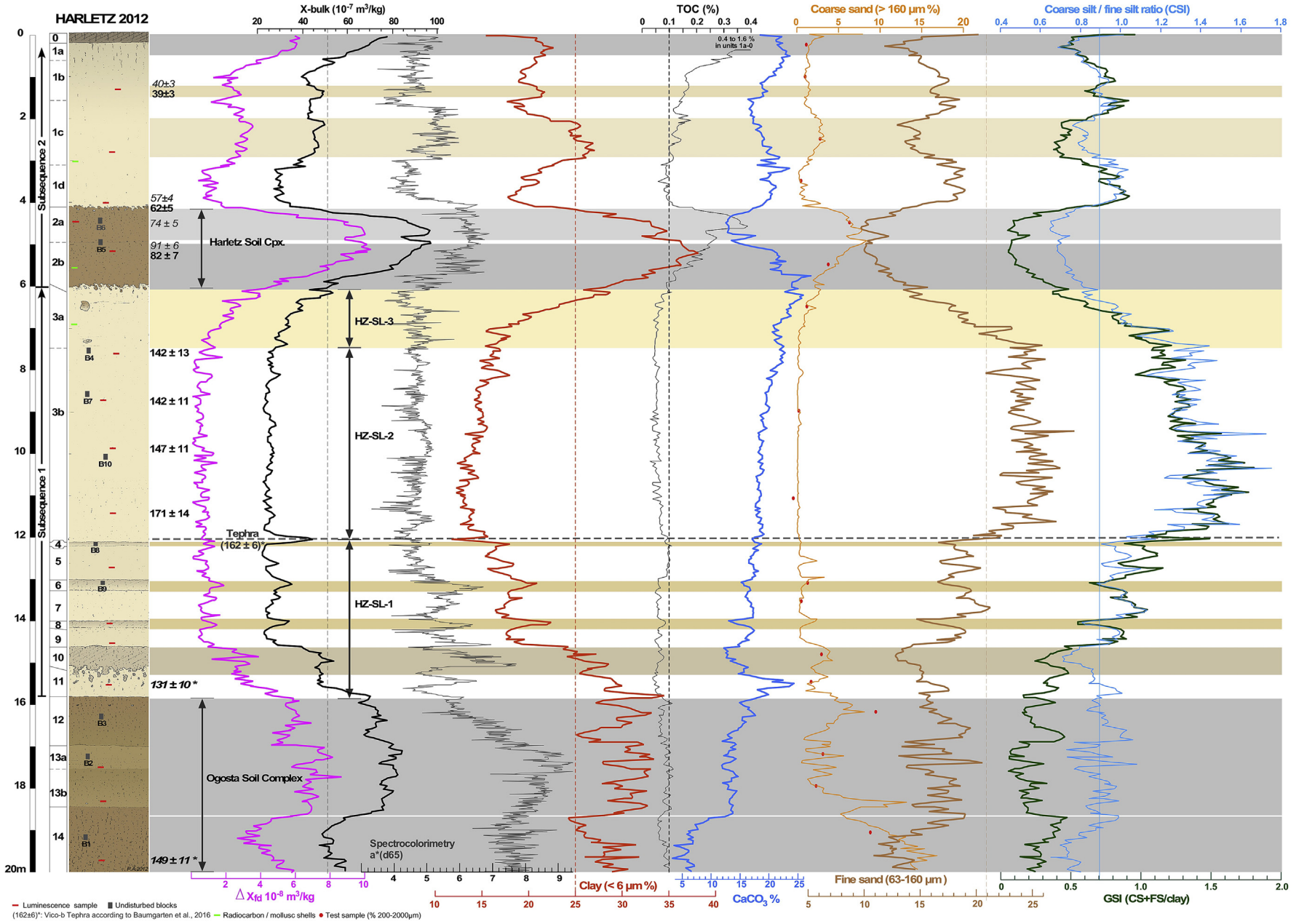

Fig. 5. Detailed stratigraphic log of the Harletz profile including the location of the various luminescence and micromorphological samples (blocks). High-resolution grain size data (clay, coarse and fine sand, grain-size ratios (GSI and CSI), TOC, carbonate, mass-specific magnetic susceptibility (χ_{BULK} in 10^{-8} m^3/kg) and absolute frequency dependence of mass-specific magnetic susceptibility ($\Delta\chi_{FD}$ in 10^{-8} m^3/kg), colour reflectance data and luminescence dating results from Lomax et al. (2019)) (black: feldspar coarse grain fraction, applying the MET-pIRIR protocol, grey italics: quartz fine grain fraction and SAR protocol).
Detailed description of the units: see Table 1.

Table 1
Stratigraphy of the Harletz loess sequence: description of the Units and pedosedimentary interpretation, from top to bottom.

Units	Description (field and thin sections)	Pedosedimentary interpretation
0	Brown greyish to blackish sandy silts with granular structure and numerous fine root tracks. Sharp basal contact. In a lateral profile, the base of this horizon is strongly bioturbated by numerous tacks of burrowing animals (about 5 cm in diameter).	Ploughing horizon of the surface Chernozem soil (topsoil). In a lateral profile, this horizon is thicker (0.4 m), darker, and corresponds to an in situ Ah horizon of Chernozem.
1a	Light brownish calcareous sandy silt with abundant root tracks and biogalleries with black clayey coatings and large burrows up to 5 cm in diameter.	Upper part of loess Unit 1b with abundant bioturbations originating from the topsoil. Evidences of weak pedogenic processes (higher χ_{BULK}/TOC and clay values) prior to topsoil formation.
1b	Light brown calcareous sandy silt with numerous root tracks and biogalleries with black clayey coatings and burrows up to 5 cm in diameter. Scattered little $CaCO_3$ concretions ("loess dolls" ≤1 cm) between 0.8 and 1.1 m depth.	Sandy loess strongly affected by bioturbation resulting from the biological activity of the surface soil (Cca calcic horizon of the eroded surface soil)
1c	Light brown calcareous sandy silt with numerous root tracks and biogalleries with black clayey coatings.	Weakly weathered sandy loess (mainly evidenced by grain size, spectro-colorimetry and χ_{BULK} parameters), polluted by recent bioturbations infilled by clayey-humic coatings originating from the surface organic horizon
1d	Pale light brown homogeneous calcareous sandy silt with scattered root tracks and biogalleries with dark clayey coating (insects/earthworms). In depth, this unit appears less and less affected by bioturbations. Small calcareous concretions (≤2 cm) at the base.	Typical calcareous sandy loess polluted by recent bioturbations (insect galleries), partly infilled by clayey-humic coatings originating from the surface organic horizon.
2a	Brown to brown greyish compact clayey sandy silt with strong granular structure (2–3 mm), apparent coarse sand grains (1–2 mm). Abundant fine roots porosity (≤1 mm) and mollusc shells. Bioturbated upper limit with large galleries (crotovinas) in the upper 10–15 cm. Discontinuous small stone line (≤5 mm) at the basal boundary with 2b. TOC: 0.4 %.	B-horizon of steppe soil intensely bioturbated and developed on colluviated coarse sandy silts. This horizon corresponds to an argic to cambic horizon of a luvic Cambisol (or luvic Phaeozems) (FAO-UNESCO, 2014).
2b	Brown to brown greyish compact clayey sandy silt with strong coarse granular structure and aggregates (2–5 mm) and « crunchy facies ». Abundant *in situ* fine porosity (≤ 1 mm) roots and bioturbations (1–2 mm) by insects (and earthworms?). Strong secondary $CaCO_3$ accumulation in the lower 30 cm (matrix and nodules ≤ 1 cm). $CaCO_3$ up to 20–25%. Lower boundary strongly bioturbated with large galleries excavated by burrowing animals into the underlying loess (diam.: 5–10 cm).	B-horizon of intensely bioturbated steppe soil developed on sandy loess. This horizon corresponds to an *in situ* Bv horizon of a Cambisol, the intensity of which appears in thin section stronger than in the overlying Unit 2a.
3a	Light grey brown homogeneous calcareous sandy silt with numerous scattered mollusc shells (6–7 m). Some large burrows with loess infilling. Biogalleries with clayey-humic coatings originating from the soil horizon 2b. Upper 0.5 cm very rich in secondary carbonate (matrix) and concretions ($CaCO_3$: 20–24%).	Calcareous sandy (fine sands) loess, with weak (incipient) syn-sedimentary pedogenesis developed prior to the overlying 2b soil), indicated by sedimentological and magnetic parameters (clay-TOC- χ_{BULK}). Strong secondary $CaCO_3$ accumulation in the upper 0.5 cm (Cca horizon of soil 2b).
3b	Light brown to yellowish homogeneous calcareous sandy silt with rare thin (1–2 mm) and discontinuous sandy laminations between 10.5 and 12 m. Although not visible during field works a tephra layer has been identified in this unit by magnetic parameters at −12 m depth, see: 4.1.2.1.2)	Typical calcareous sandy loess (fine sands) with high accumulation rate.
4	Light brown to light greyish brown massive calcareous sandy silt with strong fine root tracks porosity (≤1 mm), pseudomycelium, little Fe-Mn concretions and Fe-Mn coatings on biogalleries.	Incipient (embryonic) humic soil horizon (rooting Hz. with lowering of the loess deposition rate).
5	Light brown massive homogeneous calcareous (fine) sandy silt.	Typical homogeneous sandy calcareous loess
6	Light brown to light greyish brown massive calcareous sandy silt strong fine root tracks porosity (≤1 mm), pseudomycelium, little Fe-Mn concretions and Fe-Mn coatings on biogalleries. Bioturbated basal contact with Unit 7.	Incipient (embryonic) humic soil horizon (rooting Hz. with lowering of loess deposition rate). The weathering appears more developed than in the incipient soil of Unit 4.
7	Light brown massive homogeneous calcareous (fine) sandy silt.	Typical homogeneous sandy calcareous loess
8	Light brown to light greyish brown massive calcareous sandy silt with strong fine root tracks porosity (≤1 mm), pseudomycelium, little Fe-Mn concretions and Fe-Mn coatings on biogalleries, diffuse lower boundary.	Incipient (embryonic) humic soil horizon (rooting Hz. with lowering of the loess deposition rate). The weathering intensity appears more or less the same than in the incipient soil of Unit 6.
9	Light brown massive homogeneous calcareous (fine) sandy silt with scattered pseudomycelium and numerous Fe-Mn concretions (≤ 1 mm) in the upper 20 cm.	Typical homogeneous sandy calcareous loess with more marked rooting evidences.
10	Homogeneous brown to grey brownish sandy silt with fine granular structure. Abundant fine root tracks (≤1 mm), pseudomycelium and little Fe-Mn concretions and Fe-Mn coatings on biogalleries. Strongly bioturbated lower boundary (30 cm) with large burrows (5–10 cm).	Steppe soil horizon (cambic Hz.?) markedly more developed than Units 4, 6 and 8 showing a strong bioturbation by burrowing animals at the base.
11	Light brown to whitish massive sandy calcareous silt with numerous $CaCO_3$ concretions and deep calcium carbonate impregnation on root tracks ($CaCO_3$: 22–24%). Numerous large biogalleries filled by material originating from the overlying soil horizon.	Homogeneous sandy calcareous loess enriched in $CaCO_3$ in relation to the overlying soil of Unit 10 (calcic horizon Cca) and deeply bioturbated by burrowing animals.
12	Brown compact clayey coarse sandy silt weakly calcareous ($CaCO_3$: 12–15%), with diffuse granular structure, scattered mollusc in the upper part, including debris of large terrestrial species (*Cepaea* sp.). Strong bioturbation with very abundant biogalleries and casts. A few discontinuous sandy layers. Very progressive transition with the underlying level 13a.	Fluvial sandy clayey (overbank deposits) with a well developed pedogenesis (cambic horizon) and strong bioturbation by insects and earthworms (upbuilding / aggrading soil of alluvial plain).

2.3. Spectrocolorimetry

Spectrocolorimetry enables to quantify colour changes, not perceptible with the naked eye, through the acquisition of very high-resolution colour reflectance spectra (e.g.: Unit 1b, Fig. 5). The low purchase and maintenance costs and especially the portability of some spectrocolorimeters enables analyses to be acquired directly in the field and has been shown to be a powerful tool in combination with sedimentological observations (see Debret et al., 2011 for a review). At present, the CIELAB system more commonly referred to as L*a*b* system is the most widely used approach in sedimentology to report colour reflectance spectra data. The colour space it defines can be visualised in a spherical coordinate system where each of the three axes represent one of the three variables:

Table 2
Percentages of the five main grain size classes (from clay to coarse sand) for a set of 17 reference samples analysed using the classical sieving and pipetting method.

Sample depth (cm/top)	Clay (%) (<2 μm)	Fine silt (%) (2–20 μm)	Coarse silt (%) (20–50 μm)	Fine sand (%) (50–200 μm)	Coarse sand (%) (200–2000 μm)
22.50	21.5	26.3	37.8	13.3	1.1
102.50	18.9	23.6	41.2	15.3	1.0
252.50	21.3	26.7	35.3	13.9	2.8
352.50	20.1	25.1	38.2	16.1	0.5
452.50	29.2	23.7	28.0	12.7	6.4
552.50	31.5	24.2	28.1	12.4	3.8
652.50	19.2	23.3	39.0	17.3	1.2
902.50	13.1	19.8	45.0	21.9	0.2
1112.5	11.7	18.5	48.2	21.4	0.2
1312.5	19.7	22.2	38.4	18.4	1.3
1357.5	15.2	23.3	43.3	17.7	0.5
1482.5	22.1	25.0	34.6	15.3	3.0
1552.5	24.9	24.0	32.0	17.4	1.7
1622.5	27.9	20.5	25.0	17.0	9.6
1722.5	27.6	18.5	29.4	21.4	3.1
1802.5	27.1	18.9	29.7	22.0	2.3
1902.5	28.9	18.1	29.3	14.2	9.5

lightness (L*) ranging from 0% to 100%, green − red chromaticity (a*) where green is negative and red is positive, and blue − yellow chromaticity (b*) where blue is negative and yellow is positive. All the data (Fig. 5) were acquired with a Minolta CM 2600d over the extended visible wavelength domain from 360 to 740 nm and operating with a 6504 K light source. The sensitivity of the device allows wavelength spectrum resolution of 10 nm. The a* parameter tracks variations related to the redness of the sediment (Fig. 5) and was postulated by Ji et al. (2004) to proportionally vary with hematite of pedogenic origin associated with clays. In the present study, we combine a* with clay percentage, magnetic susceptibility values and thin sections observations, where a* is considered as a proxy of the intensity of the weathering and of soil formation processes.

Measurements in the field were conducted at a 1 cm depth resolution. For the purpose of comparing spectrocolorimetry data with other proxy data acquired along HZ12 at a 5 cm depth resolution bulk samples, the variables a*, b* and L, across a bulk sample interval (n = 5), were averaged and their standard deviation calculated.

2.4. Magnetic susceptibility

The in-field volume-specific magnetic susceptibility (κ_{FIELD}) was measured with a handheld KT-6 Kappameter from SatisGeo (Brno, Czech Republic) along the entire section at a 10 cm depth interval. Five measurements were made evenly spaced across approximately 1 m in width at each stratigraphic level. Mean values and standard deviations were calculated. Laboratory measurements of the mass-specific magnetic susceptibility (χ_{BULK}) was analysed on the bulk samples at a 5 cm depth interval with a Bartington MS2B dual frequency bridge operating with a field amplitude of 200 A/m and at frequencies of 465 Hz and 4650 Hz. Bulk material was homogenized and compacted in 8 cm^3 plastic boxes. The absolute frequency dependence of magnetic susceptibility ($\Delta\chi_{FD}$) is the difference between the low-frequency and the high-frequency mass specific magnetic susceptibility. $\Delta\chi_{FD}$ is a measure of the concentration of magnetic particles of grain size near the superparamagnetic (SP) to stable single domain (SSD) threshold at room temperature (30 nm). Within a loess and palaeosol sequence magnetic particles of this size are considered to be of pedogenic origin (Maher and Taylor, 1988; Zhou et al., 1990) and $\Delta\chi_{FD}$ is expected to increase with increasing degree of pedogenesis if mean annual precipitation does not exceed 1200–1500 mm/yr (Thompson and Maher, 1995; Balsam et al., 2011) and in the absence of other diagenetic alteration process (e.g. Taylor et al., 2014).

2.5. Luminescence dating

16 samples were taken at night for luminescence dating, by scraping unexposed sediment into black plastic bags (e.g. Fuchs et al., 2013). It was attempted to avoid areas affected by bioturbation, although this was nearly impossible in the upper part of the section. Consequently, some mixing of layers of different sedimentation ages is to be expected in the upper 1.5 m of the section. Additional samples were taken from the surrounding sediment for dose rate determination, comprising representative material within a 30 cm radius around the luminescence sample.

Samples for luminescence dating were prepared by separating the fine grain quartz fraction (4–11 μm) and the coarse grain potassium feldspar (K-FS) fraction (63–200 μm). Sample preparation for both separated fractions is described in Lomax et al. (2014a). All measurements were performed on a Lexsyg Research Luminescence reader (Lomax et al., 2014b).

The fine grain quartz samples were analysed using a standard SAR protocol (Murray and Wintle, 2000, 2003), with preheat and cutheat temperatures set at 220 and 200 °C respectively. Coarse grain feldspar samples were measured using the MET-post-IR-IRSL (MET-pIRIR) protocol (Li and Li, 2011).

Radionuclide concentrations of U and Th were determined using alpha counting and K concentrations using ICP-OES. These analyses were carried out at the University of Bayreuth (Department of Geography). For further details, see Lomax et al. (2019).

2.6. Radiocarbon dating protocol of gastropod shells

Land snail shells (*Helicopsis striata)* were slightly crushed in an agate mortar. All samples were leached with 0.01M HNO_3 at room temperature for at least 30 min and rinsed with Milli-Q water to remove superficial contamination and oxidize any remaining organic matter. Extra water is removed using a Pasteur pipette. Samples were then introduced into the bottom of a two-fingers reactor (Tisnérat-Laborde et al., 2001) and 1 cm^3 of pure H_3PO_4 (100%; previously distilled for 3 days at 105 °C and stored under argon) is added into the lateral reservoir. The reactor with the wet sample and H_3PO_4 is rapidly connected to the semi-automated vacuum line. The sample is then dried on the line, and the reactor is manually rotated to pour H_3PO_4 onto the samples. Subsequent steps are: CO_2 evolving, water elimination, and evaluation of C quantity. CO_2 reduction and ^{14}C activity measurements are performed in Saclay (Cottereau et al., 2007). Results are expressed according to Stuiver and Polach (1977).

3. Results

3.1. Stratigraphy

The detailed pedostratigraphic study of the profile describes a sequence composed of 14 main units over the 20 m of its thickness (Fig. 5). Some of the main micromorphological features from the various soil horizons and loess layers are shown in Fig. 6. From the top to the base, the pedostratigraphic sequence of Harletz is described in Table 1.

3.2. Sedimentology

Results of the grain size analysis are presented in Fig. 5 along side of the stratigraphic log and summarised through data profiles of clay (≤6 μm) percentages, CSI, GSI, fine sand (63–160 μm) and

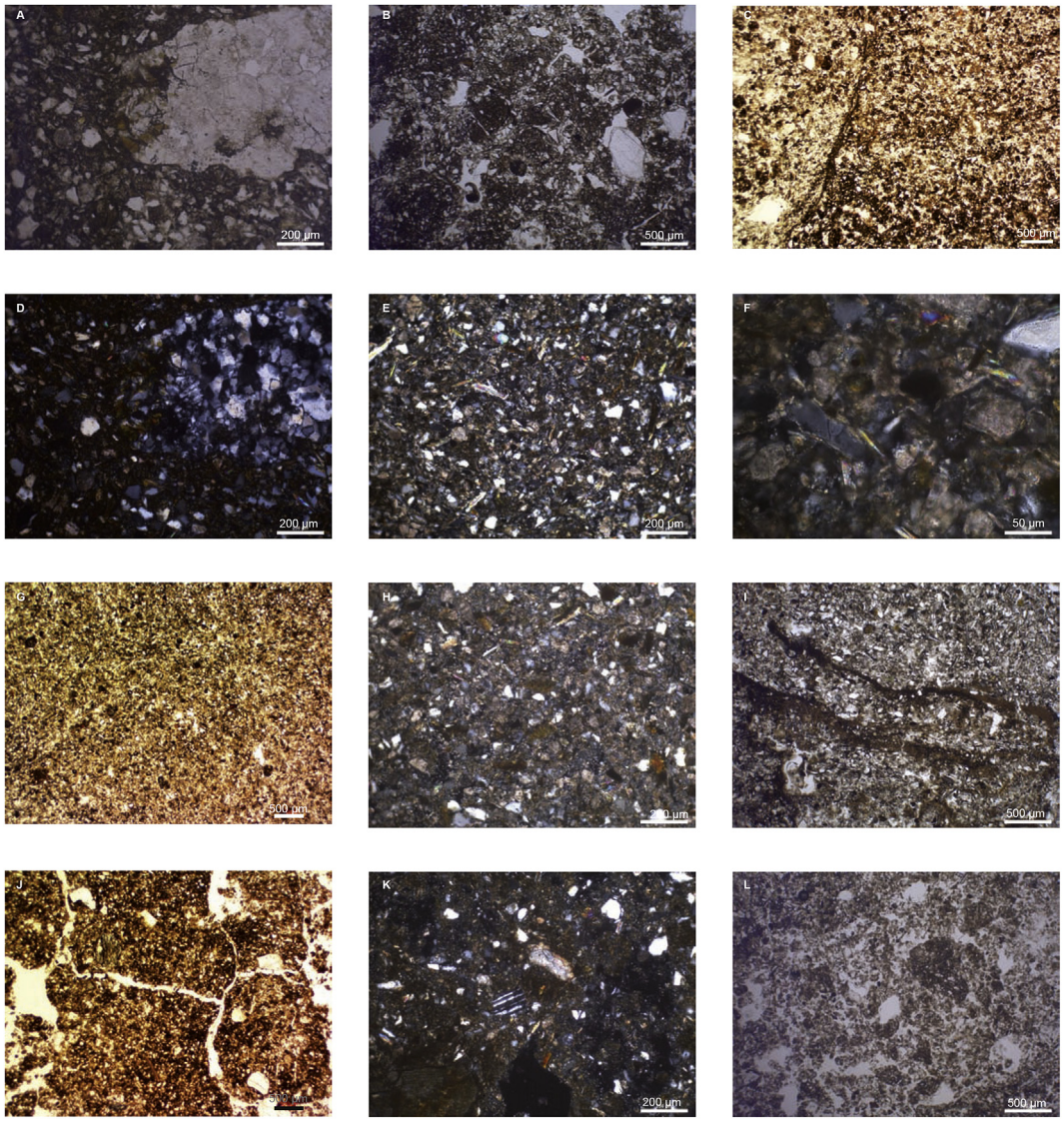

Fig. 6. Micromorphology description of Harletz thin sections (location of samples: see Fig. 5)
A to D: Ogosta Soil Complex
A and D: sample B3 – rock fragment, PPL and XPL;
B: sample B3 – The sediment consists mainly of quartz silt and sand. Muscovite and other minerals are abundant. No visible bedding. The sediment is strongly bioturbated with a channel microstructure, and rounded aggregates. Biological cavities can exceed a few centimeters in diameter.
C: sample B2 – On the left, vertical biological channel intersecting the bedding on the right. The sediment consists essentially of quartz sand and silt, with numerous muscovite and other minerals. The bedding is of sedimentary origin. The walls of the channel are lined with fine particles.
E to I: Lower loess (Unit 3b and 4)
E and F: sample B8 – Calcareous loessic deposit. Channels are numerous but very small, less than a few millimetres long. E: quartz silt, micas (muscovite and biotite) and carbonates. F: detail of carbonates grains.
G to I: sample B4 - Calcareous loessic deposit. G: The sediment is much less bioturbated than in B8. Weak channel microstructure. No aggregates, PPL. H: quartz and calcite grains; numerous micas, XPL; I. bioturbation with silty deposit, PPL.
J to L: Harletz Soil Complex
J and K: sample B5. J: quartz silt and sand; mainly porphyric related distribution; subangular blocky microstructure, mixed with channel and chamber microstructure; in chambers, granular microstructure (pellets). No coatings. K: in the middle, feldspar.
L: sample B6 - Mainly enaulic related distribution, locally a tendency to chitonic or porphyric related distribution. Granular microstructure probably resulting from biological activity, mixed locally with blocky microstructure. Numerous little channels, for most of them empty.

coarse sand (>160 μm) percentages. Overall, we note a very good correlation between the structures recorded by the various sedimentological parameters and the pedostratigraphy, even at the scale of very thin units as the micro-soil of Unit 6 (Fig. 5). The detailed description of these variations regarding to the pedostratigraphic succession is included hereafter in the first part of the discussion (part 4.1).

3.3. Magnetic susceptibility

Profile data of laboratory analyses of magnetic susceptibility (χ_{BULK} and $\Delta\chi_{FD}$) are plotted in Fig. 5 along side the stratigraphic log of the Harletz sequence.

The large-scale variations observed in the κ_{FIELD} data (see Fig. 2 in Lomax et al., 2019) are reproduced in the higher resolution laboratory data in which finer-scale structures are revealed. The two welded soils of Unit 2 are well resolved as well as the series of incipient soils of Units 4, 6, and 8. Of these, only Unit 6 is observed in κ_{FIELD}. χ_{BULK} ranges from minimum values of 25×10^{-8} m^3/kg across the lower and middle parts of loess Unit 3 to maximum values of 100×10^{-8} m^3/kg at the top and base of palaeosol Units 2b and 2a, respectively (Fig. 7). In a previously studied section located a few hundred of meters away on a carved cliff face of a downstream meander of the paleo-Ogosta river (Avramov et al., 2006), χ_{BULK} values across the prominent Unit 2 palaeosols peaked at 50×10^{-8} m^3/kg, which is half of HZ12 values. Indeed, Avramov et al. (2006) reported the occurrence of an incipient soil at an equivalent stratigraphic depth to HZ12 Unit 2. Otherwise, the reported data for these two proximal sections describe similar variations and both capture the sharp increase in χ_{BULK} at the base of Unit 3 (ca. 13 m depth in Avramov et al., 2006 section).

Pedogenic neo-formation of iron oxides may be tracked with $\Delta\chi_{FD}$ and $\%\chi_{FD}$ where their magnitudes are generally proportional to the relative concentration of superparamagnetic (SP) particles (Dearing et al., 1997). It is however noteworthy to remember that the magnitude of $\%\chi_{FD}$ is also dependant on magnetic grain size distribution where for the same absolute concentration of SP particles but having a grain size distribution of greater width will have a lower $\%\chi_{FD}$ (Eyre, 1997). Along HZ12, the mean $\Delta\chi_{FD}$ is $3.10 \pm 2.67 \times 10^{-8}$ m^3/kg with minimum and maximum values of 0.06×10^{-8} m^3/kg and 10.0×10^{-8} m^3/kg respectively. The mean $\%\chi_{FD}$ is $5.2 \pm 2.8\%$ with minimum and maximum values of 0.2% and 11.0% respectively. The sharp peak in χ_{BULK} at the base of Unit 3 is not coupled with elevated values of $\Delta\chi_{FD}$ and $\%\chi_{FD}$ as observed for Units 14 through 10, the upper parts of Unit 3, Units 2a and 2b, the upper two-thirds of Unit 1 and the topsoil.

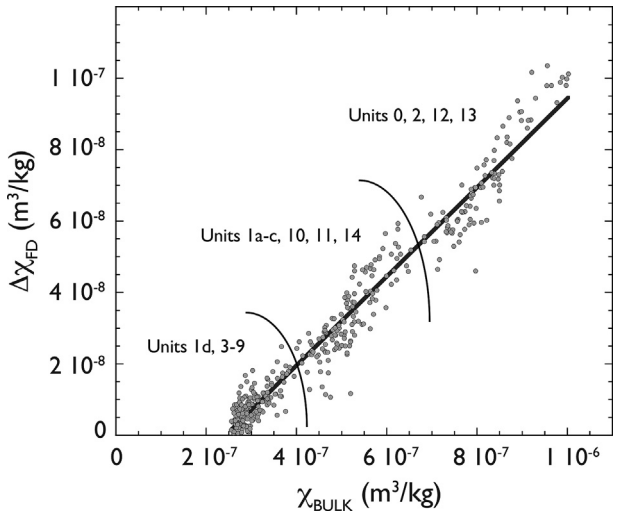

Fig. 7. A bivariate plot of the absolute frequency dependence of mass specific magnetic susceptibility ($\Delta\chi_{FD}$) and the bulk mass specific magnetic susceptibility (χ_{BULK}) of all 400 5 cm sampling depth intervals. The variables are linearly correlated with an R^2 of 0.96, a slope of 0.12 and a y-intercept of -3.02×10^{-8} m^3/kg. See Section 3.3 for discussion of results.

Plotting $\Delta\chi_{FD}$ against χ_{BULK} displays an overall linear correlation with an R^2 of 0.96 but breaks in the data distribution are evident at χ_{BULK} values of ca. 40×10^{-8} m^3/kg and 70×10^{-8} m^3/kg delimiting three groups (Fig. 7) which coincides with discrete stratigraphic units. The group with the highest values of χ_{BULK} and $\Delta\chi_{FD}$ is composed of three continuous depth intervals: 18.65–15.75 m, 5.75–4.25 m, and 0.35–0 m. These horizons correspond to the highest degree of pedogenic development within the basal fluvial soil complex (Units 13 and 12), the Harletz Soil Complex (Unit 2a-2b) and upper part of the topsoil. Moderate levels of pedogenic alterations or poor preservation of pedogenic fine-grained magnetic mineral (i.e. Unit 14) are suggested for depths with mid-range values of χ_{BULK} and $\Delta\chi_{FD}$. The moderately altered loess depth intervals are: 15.75–14.60 m (Units 11 and 10), 6.65–5.75 m (upper part of Unit 3a and lower part of Unit 2b), 4.25–4.10 m (top of Unit 2a), 3.15–0.35 m (Units 1c, 1b, and 1a). Low $\Delta\chi_{FD}$ values are associated with the least altered or pristine loess intervals with equally low χ_{BULK} and clay percentages (Fig. 8B) and unimodal grain size curves (Fig. 9A). Unaltered loess deposits are preserved over two continuous depth intervals, 14.50–6.65 m and 4.10–3.15 m, but excludes the 12.10–12.00 m depth interval (see below and Section 4.2.1). The former corresponds to the loess and incipient soils of Units 9 through 4 and the massive loess of Unit 3b and the base 3a of Saalian glacial age; while the later corresponds to Weichselian age loess of Unit 1d. The incipient palaeosols (Units 8, 6, 4) and underlying loess (Units 9, 7, 5) have $\Delta\chi_{FD}$ and $\%\chi_{FD}$ that are undistinguishable from those of unaltered loess. This said small variations in χ_{BULK} and clay % do display local highs for Units 8 and 6 as well as at 12.60 m depth midway through loess Unit 5. A local high associated with the incipient palaeosol of Unit 4 is masked by the sharp peak in χ_{BULK} at the base of Unit 3. As stated above, this peak is not associated with any frequency dependence of magnetic susceptibility even though with a χ_{BULK} of 46×10^{-8} m^3/kg this layer should behave similarly to the Group 2 population. This anomalous layer is likely the result of a thin tephra fall layer or tephra material mixed in with the loess (see Section 4.2.1).

The interpretation of $\Delta\chi_{FD}$ as a proxy for the degree of pedogenesis is compared and cross-checked with clay content and a* (Fig. 8). Like $\Delta\chi_{FD}$, both clay % and a* are expected to increase with increasing degree of pedogenesis; the former as a result of mineral weathering and the latter as a result of increased reddening of the sediment. The relationship between clay % and the relative concentration of superparamagnetic particles ($\Delta\chi_{FD}$), shown in Fig. 8B, is linear with an R^2 of 0.85 and a y-intercept of 15.4%, which coincides with background clay % values across unaltered loess of Unit 3b. The relationships between a* and clay % or $\Delta\chi_{FD}$ are more complex, yet not random, and allow to further discriminate between the various pedogenic units as well as loess units (Fig. 8A, C). For example, the basal fluvial soil complex in Fig. 8C plots as three distinct modes where the mode centred on a* values of 6 correspond to Unit 12, the mode centred on a* values of 9 correspond to Unit 13, and the mode centred on a* values of 8 correspond to Unit 14.

3.4. Luminescence dating

Luminescence ages for the quartz fine grain and feldspar coarse grain fractions are shown in Table 3 and in first in Fig. 5. The reader is referred to Lomax et al. (2019) for a more comprehensive

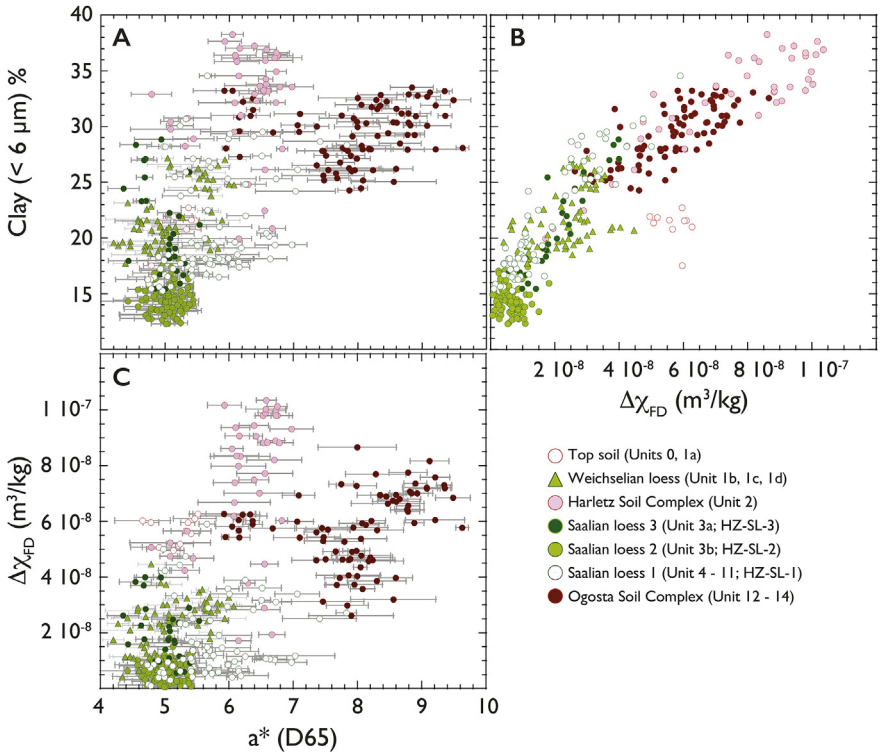

Fig. 8. Bivariate plots comparing and cross-checking three proxies (clay %, a*, and $\Delta\chi_{FD}$) of degree of pedogenesis: (A) clay % against a*, (B) clay % against $\Delta\chi_{FD}$, and (C) $\Delta\chi_{FD}$ against a*. See Section 3.3 for discussion of results.

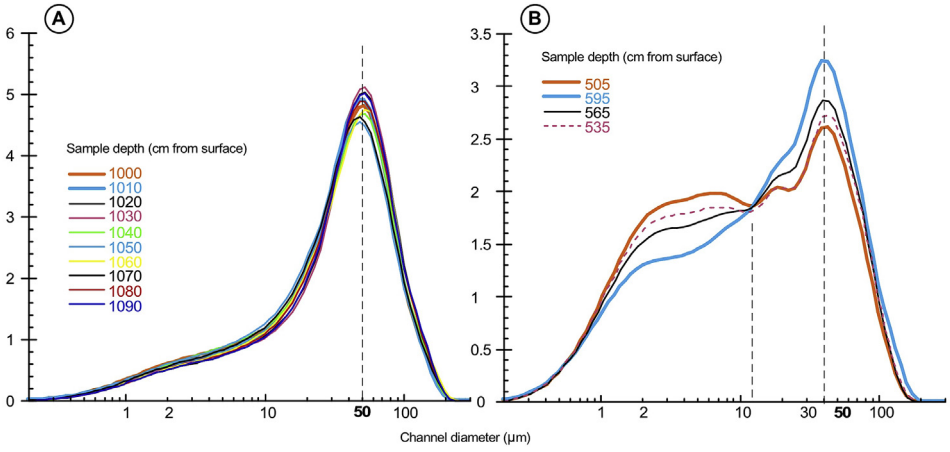

Fig. 9. Cumulative grain size curves of A: typical loess samples from Unit 3b (between 11 and 10 m) and B: samples from the lower soil horizon (2b) of the Harletz Soil Complex (between 6 and 5 m). Legend names are depths in centimetres.

reporting of Harletz luminescence ages. They demonstrated that the quartz ages for the upper part of the sequence (Unit 1a-d) and the underlying palaeosol unit are reliable, and that all older ages are underestimated, since doses in these samples exceed the saturation level of 200–300 Gy estimated by Timar-Gabor and Wintle (2013). In Figs. 5 and 10–12 we reported the four quartz ages from the upper 4.6 m of the section that are considered as reliable (italics) and the nine feldspar ages (bold) from 1.35 to 19.75 m (bold). The feldspar ages that appear strongly underestimated owing to both their position below the tephra layer (identified at 12 m by magnetic parameters and correlated with the Vico B-ignimbrite, see: 4.1.2.1.2) and their stratigraphic location regarding to the basal soil complex are in bold italic with a superscript star.

In case of the feldspar extracts, equivalent dose (D_e) determination was hampered due to the lack of a D_e plateau within the MET-pIRIR measurements for most of the samples. A pIR stimulation temperature of 150 °C showed a good match with quartz ages in the upper part of the profile. Based on this observation, all feldspar ages which build up the chronology of the lower part of the section, are based on pIR stimulation temperatures of 150 °C (Lomax et al., 2019). The two lowermost ages show an age inversion and, compared to overlying ages, appear greatly underestimated. The reason for this is unclear, but may relate to both the underestimation of the water content and overestimation of the dose rate.

Table 3
Luminescence age determinations from Lomax et al. (2019) (Q: quartz, FS: Feldspar).

Sample	Depth (m)	Unit	Water (%)	n	D_e (Gy)		U (ppm)	Th (ppm)	K (%)	Dose rate (Gy/ka)		Age(ka)	
				(Q/FS)	Q	FS				Q	FS	Q	FS
Gi05	1.35	1b	12	6/5	142 ± 5	141 ± 7	3.85 ± 0.32	9.52 ± 1.05	1.52 ± 0.08	3.56 ± 0.21	3.65 ± 0.23	*40 ± 3*	**39 ± 3**
Gi06	2.80	1c	–	-/-	–	–	3.76 ± 0.32	8.59 ± 1.00	1.47 ± 0.07	–	–	-	**-**
Gi07	4.00	1d	12	6/8	197 ± 6	217 ± 9	4.12 ± 0.29	7.59 ± 0.96	1.53 ± 0.08	3.43 ± 0.21	3.53 ± 0.23	*57 ± 4*	**62 ± 5**
Gi08	4.45	2a	15	6/-	227 ± 7	–	3.34 ± 0.30	7.48 ± 0.93	1.50 ± 0.08	3.06 ± 0.18	–	*74 ± 5*	**-**
Gi09	5.20	2b	15	6/6	267 ± 9	252 ± 14	3.26 ± 0.26	7.53 ± 0.85	1.39 ± 0.07	2.93 ± 0.17	3.07 ± 0.20	*91 ± 6*	**82 ± 7**
Gi10	7.60	3b	12	6/5	297 ± 10	485 ± 30	3.46 ± 0.28	9.07 ± 0.94	1.50 ± 0.07	3.29 ± 0.20	3.40 ± 0.22	*90 ± 6*	**142 ± 13**
Gi11	8.70	3b	12	6/4	320 ± 10	480 ± 22	3.58 ± 0.28	8.48 ± 0.91	1.50 ± 0.08	3.27 ± 0.20	3.38 ± 0.22	*98 ± 7*	**142 ± 11**
Gi12	9.90	3b	12	4/5	339 ± 13	502 ± 17	3.04 ± 0.31	10.90 ± 1.01	1.49 ± 0.07	3.30 ± 0.20	3.41 ± 0.23	*103 ± 7*	**147 ± 11**
Gi13	11.45	3b	12	-/5	–	579 ± 28	3.69 ± 0.30	8.52 ± 0.98	1.50 ± 0.07	–	3.39 ± 0.23	-	**171 ± 14**
Gi14	12.80	5	12	6/-	324 ± 13	–	3.94 ± 0.30	8.53 ± 1.00	1.60 ± 0.08	3.45 ± 0.21	–	*94 ± 7*	**-**
Gi15	14.05	8	12	6/-	339 ± 14	–	4.01 ± 0.31	8.95 ± 1.03	1.64 ± 0.08	3.54 ± 0.22	–	*96 ± 7*	**-**
Gi16	14.10	9	15	-/-	–	–	4.32 ± 0.30	7.64 ± 0.97	1.64 ± 0.08	–	–	-	**-**
Gi17	15.55	11	15	6/5	331 ± 11	429 ± 16	3.30 ± 0.33	10.62 ± 1.08	1.42 ± 0.07	3.16 ± 0.19	3.28 ± 0.22	*105 ± 7*	**131 ± 10**
Gi18	17.55	13a	20	6/-	345 ± 13	–	4.34 ± 0.29	7.15 ± 0.94	1.40 ± 0.07	2.99 ± 0.18		*115 ± 8*	**-**
Gi19	18.40	13b	20	6/-	355 ± 12	–	3.80 ± 0.27	8.29 ± 0.90	1.47 ± 0.07	2.99 ± 0.18		*119 ± 8*	**-**
Gi20	19.75	14	25	5/5	332 ± 12	469 ± 19	3.66 ± 0.26	7.61 ± 0.86	1.77 ± 0.09	2.99 ± 0.17	3.14 ± 0.20	*111 ± 7*	**149 ± 11**

The water content estimation is especially difficult for the basal soil complex (12–14) developed mainly as upbuilding soil horizons in a flood plain environment subject to regular flooding events.

4. Discussion

4.1. Pedostratigraphy and palaeoenvironments

The combination of high-resolution pedostratigraphy, grain size studies, and of additional analytical parameters (χ_{LF}, $\Delta\chi_{FD}$, colour reflectance, TOC and $CaCO_3$), throughout the whole sequence, shows a very good correlation between all proxies and the stratigraphic boundaries defined in the field (Fig. 5). Some very thin (ca. 10 cm) horizons like the micro-soils of Units 4 or 8 especially well illustrate this characteristic (Fig. 5). In addition, variations in both clay percentage and GSI, combined with parameters as a* values, TOC percentage or magnetic parameter, enable to highlight variations within the sediments which were not visible in the field despite a very detailed observation. A good example is given in the upper part of the profile (Unit 1a to 1d, Fig. 5).

From a global pedo-sedimentary point of view, the Harletz sequence appears to be composed of two main parts corresponding to two contrasted environments, from the base to the top:

1) A basal fluvial soil complex (Ogosta Soil Complex), dominated by low dynamic fluvial sedimentary processes of alluvial plain (overbank deposits), associated with more or less contemporary pedogenic processes (Units 14 to 12).
2) A loess-palaeosol sequence (LPS), dominated by aeolian sedimentation (loess) more or less sandy (Units 11 to 3b and 1d-1a), interrupted by a succession of weakly developed soils (incipient soils) at the base (Units 10, 8, 6, 4). This sequence is divided in two parts by a well-developed 2 m thick soil complex (2a-2b Units, Harletz Soil Complex) and is overlaid by a strongly truncated topsoil (Unit 0).

4.1.1. Basal fluvial soil complex (Ogosta Soil Complex) (Units 14–12)

This part of the record corresponds to a thick (4.7 m) brown sandy-clayey pedosedimentary complex in which χ_{BULK} values are generally high and consistent with an environment dominated by soil formation (≥80 μSI unit). An important biological activity is attested by the abundance of earthworm diapause chambers and insect galleries filled with clay pellets and scattered mollusc shells (including large terrestrial species typical of arboreal and semi-forested environments (*Cepaea* sp., Table 4). This biological activity is however not reflected in the organic carbon that remains low (ca. 0.1%) throughout the whole basal fluvial soil complex. Moreover, the lower part of this complex (Unit 14) underwent hydromorphic processes (lower χ_{BULK}) induced by vertical movements of the water table in the Ogosta River alluvial plain that have likely partially dissolved ferrous oxides below 19 m, lowering χ_{BULK} and $\Delta\chi_{FD}$ values with respect to overlying Units 13 and 12 (Figs. 5, 7 and 8C).

Given its characteristics and location regarding to the current topography of the alluvial plain, it is proposed that the basal fluvial soil complex has formed at the margins of a fluvial system that was in a similar position to the present day Ogosta River (a few meters below the base of the present day section). Indeed, the coarse sand fraction (up to 2–4 mm particles visible in the field) shows similar characteristics (grain size and mineralogy) than coarse sands sampled from the present Ogosta River bed (grain size composition of the Ogosta river sample: silts, fine and medium sands (<0.5 mm): 20%, coarse sands (0.5–1 mm): 45%; very coarse sands (1–2 mm): 20% and fine gravels (>2 mm):15%).

This observation reflects the proximity of the palaeochannel from which these sediments have been deposited through repeated flooding episodes (overbank deposits). Field and thin section observations as well as elevated redness colour index (a*), χ_{BULK} (κ_{FIELD}) and $\Delta\chi_{FD}$ all support the occurrence of soil forming processes throughout the basal fluvial soil complex. The impact of pedogenesis is also depicted in the cumulative grain size curves that show a very developed secondary mode centred around 4–5 μm (Fig. 9B). High frequency variations in both clay percentages and χ_{BULK} values through the basal fluvial soil complex suggest that the whole complex results from upbuilding soil processes (Almond and Tonkin, 1999; Eger et al., 2012) developing (aggrading) contemporaneously with repeated and variable overbank fluvial sedimentation in the alluvial plain. Sedimentological data show however that the basal fluvial soil complex is not composed of a single upbuilding soil but by a succession of at least two distinct phases.

Finally, leaching and precipitation of $CaCO_3$ at the base of the profile produced large "loess-dolls" (4–8 cm) between 19.5 and 19 m depth (Fig. 5). The absence of strong hydromorphic imprint (no gley horizon) and the presence of terrestrial molluscs shells indicate that the soil complex originally formed on a well drained substrate and was only temporarily submerged during the strongest flooding events. According to FAO – UNESCO world reference base for soil resources (2014) these soils can be described as Bt to

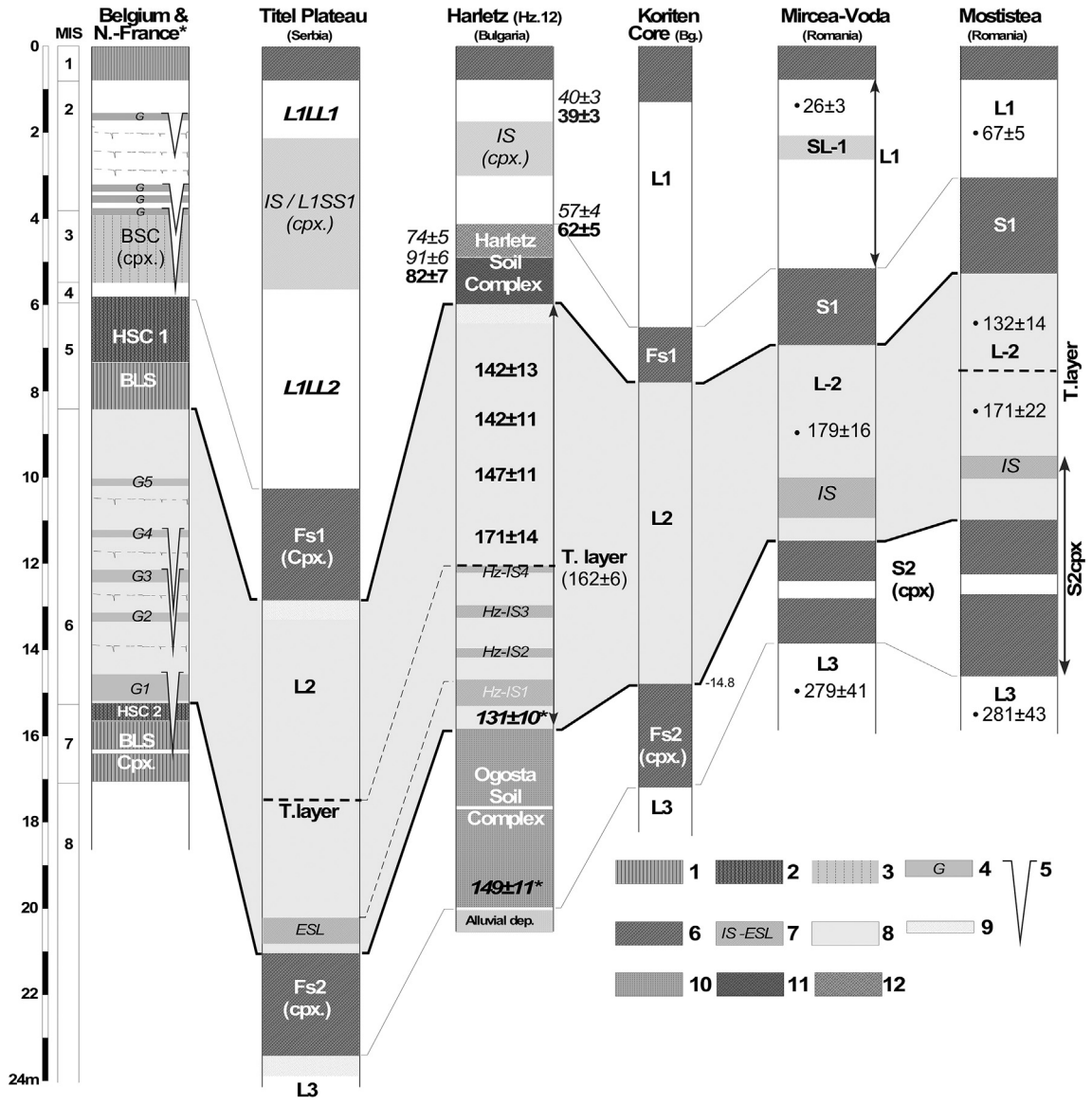

Fig. 10. Stratigraphic correlations between the Harletz sequence and some main references sequences from Serbia (Marković et al., 2015), Bulgaria (Koriten, Jordanova and Petersen, 1999), Romania (Balescu et al., 2010). Comparison with a synthetic loess-palaeosol record for North-Western Europe (France to Belgium, according to Antoine et al., 2016; Meijs, 2002).
(1 to 5: Western European sequence only).
1 Brown leached soils and soil complexes synthetic loess-palaeosol record: Bt horizon (s) of brown leached soil (s).
2 Humic soil complexes (HSC 1 and 2): grey forest soils and steppe soils complexes. 3 Boreal to arctic brown soil complex (BSC). 4) Tundra gley (G) horizons. 5) Large ice-wedge casts with loess infilling.
6) Interglacial Chernozem soil horizons. 7) Weakly developed interstadial "steppe soils" (*IS/L1SS1*): Interstadial soils and soil complexes. 8) Penultimate glacial (Saalian/MIS 6) loess. 9) Accumulation of secondary $CaCO_3$ (Cca). 10) Harletz Bt to Bw horizon of luvic Cambisols developed on alluvial sandy silts. 11) Harletz intensely bioturbated Bv horizon of interglacial Cambisol. 12) Harletz strongly bioturbated luvic Cambisol to luvic Phaeozem.

Bw horizons of luvic Cambisols.

Considering both soil characteristics (weathering, clay illuviation, prismatic structure) and intensity of the associated bioturbation indicating well-developed vegetation, it is proposed to assign this complex to an interglacial or interglacial/early-glacial context. According to: i) the occurrence below this complex of a periglacial sand and gravel body (T2 terrace), ii) the composition of the overlying pedosedimentary sequences and, iii) the MET-pIRIR results, and the age of the overlying tephra layer (ca. 12 m in Fig. 5), it is proposed to allocate this part of the Harletz sequence to the upper half of MIS 7 (MIS 7c to 7a between about 220 and 190 ka, Lisiecki and Raymo, 2005) (see Section 4.2).

Finally, if it is likely according to Varga et al. (2016) or Erhmann et al. (2017) that a proportion of Saharan dust (20–30% of the clay) has been incorporated in interglacial soil horizons, and by using their proposed values, we could expect 7.5 to 12.5% of Saharan dust in the various units in Harletz. Although it is possible that one part of the secondary mode (2–10 μm) occurring in the grain size curves of the Harletz Soil Complex (Fig. 9B) indicates an input of Saharan dust during the Last Interglacial, such a hypothesis needs to be investigated in the future by geochemical and mineral magnetism comparisons between Harletz sediment and Saharan dust samples.

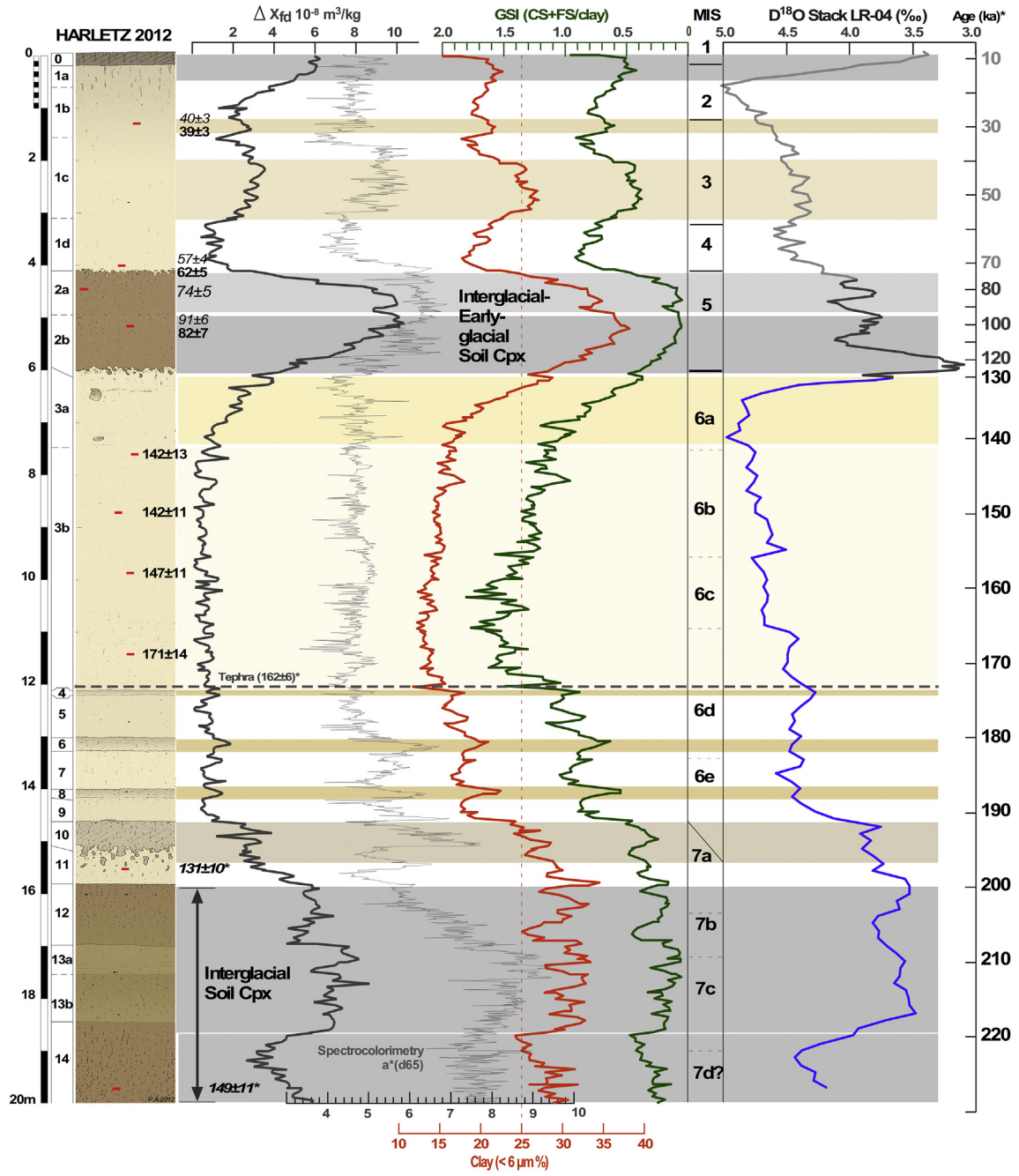

Fig. 11. Variation of absolute frequency dependence of mass specific magnetic susceptibility ($\Delta\chi_{FD}$ in 10^{-8} m^3/kg), a* (colour reflectance), clay percentages and Grain Size Index (GSI) throughout the Harletz loess-palaeosol record. Attempt of correlation with MIS stages and LR-04 Global $\delta^{18}O$ stack (Lisiecki and Raymo, 2005).
According to strong variations in sedimentation rates in the record, the LR-04 chronology has been segmented in three parts: (1) From ca.10 to 75 ka (Weichselian Pleniglacial and Late glacial) in light grey), (2) from 75 to 130 (Eemian interglacial and Weichselian Early Glacial in dark grey) and (3) from 130 to 230 (Late Saalian and younger part of the Penultimate Interglacial (MIS 7), in blue). (For interpretation of the references to colour in this figure legend, the reader is referred to the Web version of this article.)

4.1.2. Loess-palaeosol sequence (LPS)

According to field observations and analytical data, the loess-palaeosol sequence of Harletz can be divided in two subsequences (Fig. 5):

1) *Subsequence 1* includes Units 11 to 2a and is composed of a thick loess body (ca. 10 m) overlain by a well developed brown soil complex (ca. 2 m),
2) *Subsequence 2* includes Units (1d–0) and is composed of a loess complex (ca. 4 m) covered by a truncated topsoil (0–1.2 m).

4.1.2.1. Subsequence 1: lower loess and upper soil complex (Harletz Soil Complex)

4.1.2.1.1. Lower loess. A first break is observed in all proxy records between the top of the basal fluvial soil complex and the base of Unit 11 marking the beginning of both the loess sequence and Subsequence 1 (Fig. 5). These loess units are globally characterised by sandy facies (63–160 µm: 16–24%), the occurrence of an important amount of carbonates (average $CaCO_3$: 15–20% excluding layers with strong secondary carbonate accumulation) and a CSI ratio of 0.6–1 in the lower part reaching 1 to 1.6 in the

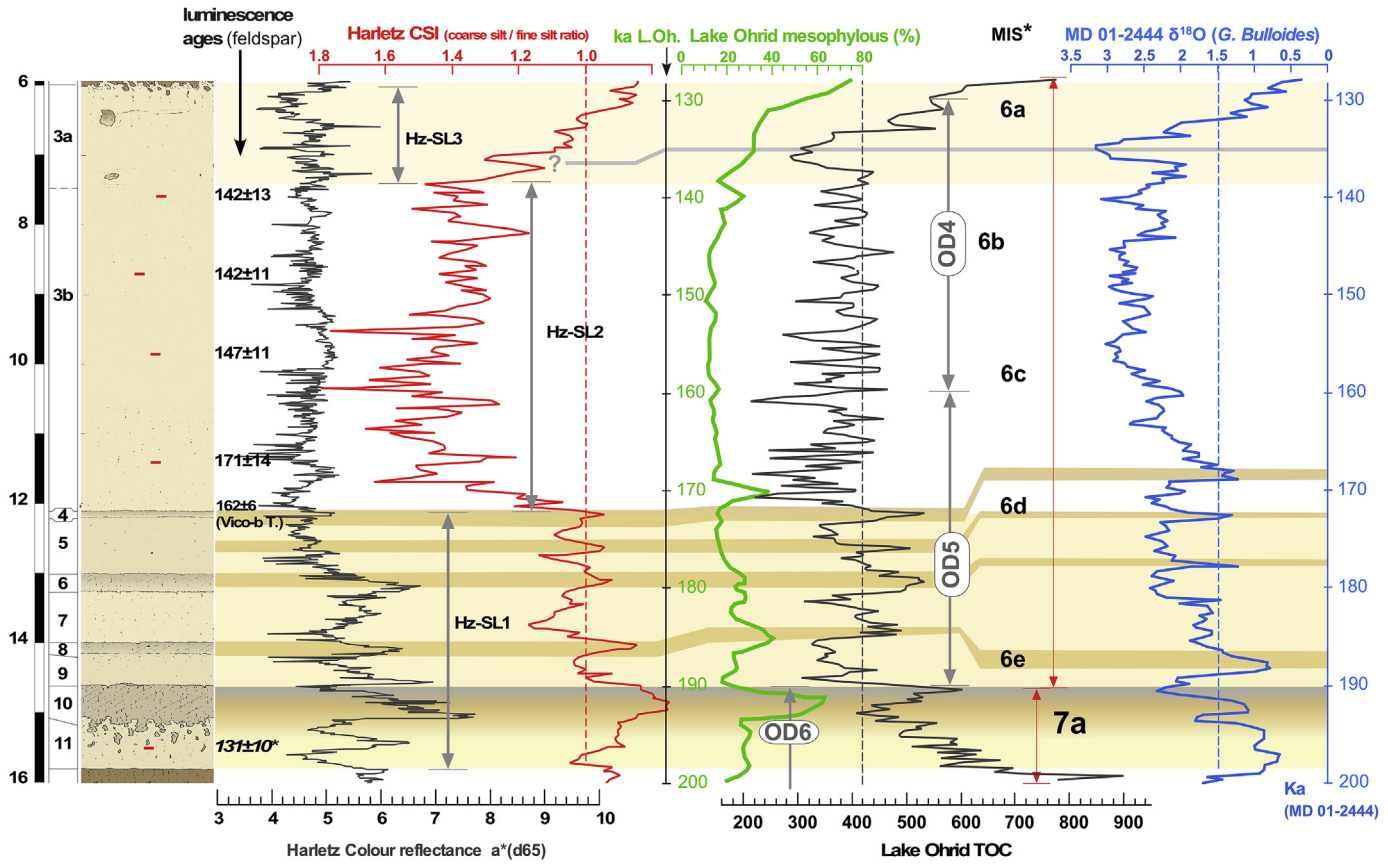

Fig. 12. Attempt of correlation between the Saalian part of the Harletz section, CSI and a* with the Lake Ohrid record and chronology (TOC and percentage of mesophylous species, according to Francke et al., 2016 and Sadori et al., 2016). Comparison with MIS stages (LR-04) and sub-stages (Railsback et al., 2015), and the high-resolution record of $\delta^{18}O$ of *G. bulloides* from Eastern Atlantic (Iberian Margin), according to Hodell et al., 2013).

Table 4
Malacological assemblages from two test samples collected in Units 2b and 12; interpretation of local environmental and climatic conditions (determination by Jitka FRODLOVA, University of Brno, Czech Republic). For each sample the species (n1 to n6) are presented by decreasing relative abundance.

Sample	Mollusc species (»> markedly dominant species)	Interpretation
HZ-12–5.9-6.0 m Unit 2b	1) »> *Cernuella* cf. *virgata* (Da Costa, 1778) 2) *Chondrula tridens* (Müller, 1774) 3) *Helicopsis striata* (Müller, 1774) or *Candidula rhabdotoides* (Wagner, 1928) 4) *Punctum pygmaeum* (Draparnaud, 1801)	Dry soil with grassland developed under a temperate (interglacial ?) climate (*Punctum pygmaeum*).
HZ 12–16.05 to –16.25 m Unit 12.	1) »> *Chondrula tridens* (Müller, 1774) 2) *Granaria frumentum* (Draparnaud, 1801) 3) *Cernuella* sp. 4) *Cepaea* sp. 5) *Helicopsis striata* (Müller, 1774) 6) *Candidula rhabdotoides* (Wagner, 1928).	Dry and well-drained environment. Relatively well-developed vegetal cover developed under interglacial conditions with some arboreal vegetation very likely (*Cepaea* sp.)

thick loess body of Unit 3a-3b. The lower part of subsequence 1 is marked by a progressive decrease over a 4 m interval in clay percentages from 24 to 26% in the basal fluvial soil complex to 10–12% in loess at 12 m depth (Unit 4). The loss of clay content is compensated by an equivalent increase in coarse-silt (25–63 μm) typical of loess deposits (Varga et al., 2012; Vandenberghe, 2013). In addition, the grain size distribution spectra define a single mode characteristic of wind blown sediments, centred at 50 μm (Fig. 9A). Magnetic susceptibility values decline more rapidly from the top of the basal fluvial soil complex, reaching average values of ca. 30×10^{-8} m^3/kg at the top of Unit 10, which are maintained low up to the top of Unit 3b.

The transition between the basal fluvial soil complex and the thick loess of Unit 3 develops over a depth of about 3.5 m, as a succession of four loess-soil cycles including Units 11 to 4. This part of the record is characterised by the alternation of pure calcareous loess deposits, becoming progressively less clayey from the base to the top (Units 11, 9, 7, 5), and of increasingly poorly developed brown to grey soil horizons from the base to the top (Units 10, 8, 6, 4). These embryonic or incipient soils are 10–20 cm thick and are very well highlighted by increases in clay content (3–4% variation), decreases in GSI, observed iron and manganese precipitates, the occurrence of pseudo-mycelium (and $CaCO_3$ depletion) and of earthworm calcite granules (see Table 1). Magnetic susceptibility values and its frequency dependence (Fig. 5), considered as a marker of pedogenesis, remain elevated in Unit 10 which appears

to be the youngest well-recorded soil horizon in this part of the sequence. This soil is also indicated by a strongly bioturbated basal boundary, a granular structure, an elevated clay content (25–28%), a slightly higher TOC %, and an important secondary carbonate accumulation in the directly underlying loess horizon (ca. 25%).

Given their characteristics, and by comparison with data from Upper Last Glacial loess sequences of Central Europe (Haesaerts et al., 2003; Rousseau et al., 2011), these embryonic soil horizons or "rooting horizons" likely reflect short episodes of a few centuries during which wind dynamics is strongly reduced allowing the development of herbaceous vegetation (steppe) in a slightly wetter environment. The decrease in pedogenic intensity observed upwards from Units 10 to 4 is indicative of a progressive aridification of the environment favourable to dust deflation and transport of aeolian material from the surrounding environment (periglacial braided river systems) of the Danube (Gabris, 1994; Gabris and Nador, 2007) and Ogosta Rivers. The cyclic alternation between loess deposition and increasingly weak pedogenesis through this part of the Harletz Lower loess reveals a step-by-step evolution towards more and more arid and full glacial conditions. This evolution could indicate a complex transition to a Pleniglacial environment similar to what has been observed in European loess sequences at the beginning of the Last Glacial period (Haesaerts and Metsdagh, 2000; Antoine et al., 2016, 2000, Schirmer, 2016).

The exceptionally developed loess Unit 3b which shows no discontinuity in the field except for some very rare and discontinuous sandy beds, corresponds to a calcareous (fine) sandy facies of loess (ca. 23% fine sands 63-160 μm-from 12 to 7.5 m depth) characterised by very low χ_{BULK} (ca. 28×10^{-8} m^3/kg) and $\Delta\chi_{FD}$ ($<2 \times 10^{-8}$ m^3/kg) values over more than 4.5 m, and extremely low TOC concentrations (<0.1%) (Fig. 5). Furthermore, variations in fine sand, coarse silt and GSI co-vary across Unit 3b indicating a common source for the two classes of particles. This is a typical observation for sequences located near a large fluvial network (Antoine et al., 2009a, 2013). In contrast, the percentage of coarse sand is close to zero between 12 and 7.5 m depth. At the transition between Units 4 and 3b, the two grain size ratios (GSI and CSI) clearly show a strong shift in the loess dynamics with GSI values between 1 and 1.7, corresponding to those described in other typical European loess series for both Upper Weichselian (Antoine et al., 2009a,b) and Saalian loess (Schirmer, 2016). In addition, within Unit 3 (6 m thick), two parts can be differentiated: a lower one (12.10–7.4 m) showing the highest GSI and CSI values of all the sequence, and an upper one where those indices gradually decrease, with an GSI passing below 1 within Unit 3a at around 7 m depth (Fig. 5). The detailed analysis of the grain size curves shows that the deposition of the thick loess body of Units 3b and 3a was subject to high-frequency cyclical variations in grain size (mainly in fine sand and coarse silt fractions that show short cycles developed over 20–30 cm in thickness). During the deposition of the Harletz Lower loess, aeolian sedimentation thus was not constant resulting, more likely, from successive dust storms of variable intensity as it has been proposed for the Late Weichselian loess in Western Europe at Nussloch (Antoine et al., 2009a).

According to magnetic susceptibility and grain size data, the upper part of this thick loess body (Unit 3a; 7.5 to 6 m) shows evidences for weak but more and more important pedogenesis upwards. This magnetic enhancement is interpreted as resulting from a progressive climatic improvement prior to the development of the following interglacial soil (Unit 2b). The occurrence of abundant mollusc shells in the upper half of Unit 3a likely indicates a more vegetated environment during the deposition of this loess unit than during the sedimentation of 3b in which mollusc shells are very rare.

According to the observations exposed above, we proposed a subdivision of the thick loess body formed by Units 11 to 3a (total thickness of 9.9 m) into 3 sub-units (Fig. 5), from the base to the top:

HZ-SL1 is characterised by lower sedimentation rates and the occurrence of 4 soil horizons (1 soil and 3 incipient soil horizons) showing a step-by-step evolution towards a drier and colder environment with higher sedimentation rates.

HZ-SL2 is showing a very thick and homogeneous accumulation of pure sandy calcareous loess without any weathering evidence, and the highest accumulation rates.

HZ-SL3 is characterised by a slight and progressive rise of weathering, likely a lower sedimentation rate with contemporaneous weak soil development (upbuilding) and a strong increase in mollusc populations.

4.1.2.1.2. Tephra layer at the base of HZ-SL2 sub-sequence. Although not visible during field investigations, a thin tephra layer has been evidenced by magnetic analyses at the base of Unit 3b at the contact with the incipient soil horizon of Unit 4. With respect to loess deposits in middle and lower Danube areas, tephra layers within the lower part of the second loess (thereafter L2) are reported for Serbia (Batajnica section, e.g. Marković et al., 2009; Osipova et al., 2013; Stalac section e.g. Obreht et al., 2016), and Romania (Mostistea, e.g. Panaiotu et al., 2001; Balescu et al., 2010) (Fig. 10). There are some magnetic indications as well for a tephra in the Kaolinovo section in northeast Bulgaria (Pers. com.: Diana Jordanova). However, source assignment of this tephra layer through geochemistry is problematic as discussed in Marković et al. (2015) because of the strong secondary alteration of the glass shards. Taking into account the identified and MIS6 dated tephra layers in lake Ohrid sequence, a probable source of the Harletz lower loess tephra could be the Vico B-ignimbrite dated at 162 ± 8 ka from the Roman volcanic province (Leicher et al., 2016). The presence of this tephra material probably could be linked to a long-range transport at that time (ca. 950 km). In view of the lateral pattern of identified tephra in L2 loess (Marković et al., 2015), it can be assigned to high altitude west-southwest winds.

According to the location of the tephra layer at the very base of the thick loess body of HZ-SL2 and the MET-pIRIR dates, the full loess body formed by Units 11 to 3a is allocated to the Late Saalian or MIS 6 (191-130ka). This allocation is also strongly supported by the location of this loess unit below the first interglacial soil (complex) occurring from the surface (Figs. 10 and 11) and by luminescence ages (Lomax et al., 2019).

4.1.2.1.3. Interglacial soil complex (Harletz Soil Complex). At the top of the Late Saalian loess of Harletz, a thick complex (6–4.10 m depth) of brown to brown-greyish bioturbated palaeosols showing a strong granular structure has developed. The complex is divided into two units visible in the field as well as in sedimentological and χ_{BULK} data (units 2a-2b). The lower horizon (Unit 2b) is characterised by a gradual increase in clay percentage reaching 32–35% in its upper part. Above the limit underlined in the field by a thin and discontinuous stone line, the upper horizon (Unit 2a) shows lower clay content with values decreasing to 24–25% at its upper limit. Moreover the pedo-facies analysed both in the field and through thin sections (Fig. 6J–L) reflects the formation of a well-developed soil: strong weathering of minerals, deep clay impregnation of the matrix, intense bioturbation (Fig. 6). The high degree of pedogenesis is also depicted by the addition of a second mode in cumulative grain size curves centred on 4–5 μm, contrasting with the unimodal distribution of unaltered loess sediments (Fig. 9B). The upper part of the Unit 2b palaeosol has then been partly eroded as evidenced by the discontinuous small stone line observed at the boundary between 2b and 2a.

The intense bioturbation that characterizes the palaeosol of Unit 2b, and the presence of secondary $CaCO_3$ as scattered small

concretions, are typical of a pedogenesis under relatively dry continental and temperate climate and a forest-steppe vegetation (Phaeozems according to FAO-UNESCO, 2014). The preservation of mollusc shells throughout the whole soil complex ($CaCO_3 \geq 15–20\%$) and the occurrence of small calcareous concretions scattered in Unit 2a also testify for a continental climate and relatively weak annual precipitation. Given the intensity of the pedogenesis revealed by the clay concentrations and the very high values of magnetic susceptibility (ca. 100×10^{-8} m^3/kg), palaeosol 2b formed under full interglacial conditions. According to its stratigraphic position, this interglacial is allocated to the Last Interglacial (MIS5e or Eemian). The ^{14}C age determination obtained from mollusc shells collected at 5.65 m severely underestimates the true age likely due to the limit of the radiocarbon dating method (Table 5).

The upper palaeosol horizon (Unit 2a), less structured than 2b and where the magnetic susceptibility values and clay content decrease continuously upward, displays a vertical inverse mirror image of the variation in depth of the physical properties of an in situ soil. It is thus likely that Unit 2a corresponds to a slow and gradual reworking of Unit 2b by colluvial processes, in a context of a relative climatic degradation during which aeolian sedimentation is also active and soil formation processes weakens. However, compared to the underlying soil, palaeosol 2a shows a markedly better preservation of the humic matter with a TOC concentration reaching 0.4% in its middle part (by far the highest value of the profile as a whole). This last point indicates an evolution of the climate towards dryer conditions allowing the preservation of organic matter in the profile, which could take place during a transition period (Early Glacial MIS 5–4?). Although only based on one quartz SAR age (74 ± 5 ka) Lomax et al. (2019), the geochronological control supports this idea.

Surprisingly, Units 2b-2a are also characterised by a high concentration of coarse sands (5–7%) significantly anti-correlated with the fine sands (Fig. 5). These coarse sands are easily visible when conducting wet sieving tests of malacological samples over a 500 μm mesh. The mineralogy and grain size of the coarse sand are similar to that of present-day sands collected from the Ogosta River bed (see above). This suggests that an additional proximal source (tens to hundreds of meters) was active during the deposition of loess sediments on which developed the interglacial palaeosol 2b (see section 4.2 for further discussion).

4.1.2.2. Subsequence 2: upper loess and topsoil. In the field, the upper part of the sequence of Harletz (Units 1d-1a) shows a particularly monotonous record, partly due to strong desiccation even though the section face was excavated 1 m or more inwards. Contrastingly, sedimentological analyses, magnetic properties and colour reflectance show significant variations, strongly correlated with each other (Fig. 5).

Two horizons with low degree of pedogenesis are thus evidenced within the loess Unit 1. The first horizon, within Unit 1c, ranges between 3 and 2 m depth (relative variation of clay content: 7%). The second horizon, within Unit 1b, from 2 to 1.5 m depth, is thinner and shows a lower degree of alteration (relative variation of the clay content: 2–3%). These observations are important for the interpretation of the sequence because they indicate that the upper 4 m of loess of Unit 1, although thinner than the loess Unit 3, does not necessarily correspond to a shorter phase of deposition. On the contrary, they rather correspond to a complex and long climate history corresponding to a succession of stadial and interstadial phases. The stadial phases are characterised by maximum GSI values and minima in magnetic susceptibility, clay content and a* values.

OSL and ^{14}C ages allow to allocate this part of the profile to the Last Glacial period (Weichselian) indicating a very low sedimentation rate for this period (4 m/60–50 ka). This results in smoothed variation in the various analytical data, mimicking the variations of the LR-04 global stack for deep-sea records (Lisiecki and Raymo, 2005) in accordance with the chronological interpretation proposed above (Fig. 11). According to this interpretation, the horizons showing weak pedogenesis in Units 1c and 1b, correspond to loess deposited during the Middle Pleniglacial (mainly MIS 3) in a particularly arid environment and unfavourable to soil development as compared with Serbian profiles (Antoine et al., 2009b). The results of the OSL (Table 3) and ^{14}C age determinations (Table 5) are consistent with this interpretation.

Finally, if the topsoil has been eroded at the main profile, a lateral section located 30 m to the Northeast allowed to describe a more complete profile, 1.5 m thick including a typical humic horizon of chernozem with a strongly bioturbated lower boundary (rodent burrows, earthworm tubules) and a calcium carbonate horizon (not described in this paper).

Table 5
Radiocarbon analysis of mollusc shells (*Helicopsis striata*).

Sample ref.	Depth (m)	Lab. Ref.	Age yr. BP (1sigma)
Hz 3.0–3.1	3.0–3.1	GifA-14362/SacA-40166	35270 ± 190
Hz 5.6–5.7	5.6–5.7	GifA-14363/SacA-40167	36840 ± 220
Hz 6.8–6.9	6.8–6.9	GifA-14364/SacA-40168	37490 ± 190

4.2. Correlations and regional significance of the record

Using a cyclo-stratigraphic approach of the sequence combined with dating constraints provided by both luminescence ages and the occurrence of the tephra layer at 12 m depth, the Harletz section exhibits a remarkably high-resolution Late Saalian (MIS6) loess accumulation in Europe (L2 loess) (Fig. 10). Indeed, if similar values have been reported from the Serbian sequences of the Titel Plateau area (8.2 m, Marković et al., 2015), from the Koriten core of NE Bulgaria (7 m, Jordanova et al., 2007) or in some west European profiles as at Kesselt in Belgium (7–8 m, Meijs, 2002) or Achenheim in France (ca. 8 m, Lautridou et al., 1985), other Danubian profiles, especially in Romania, show a markedly lesser L2 thickness (4.5–6 m including an interstadial soil in the lower part) (Fig. 10).

Looking for regional references for the basal fluvial soil complex (Ogosta Soil Complex), the closest and best-dated high-resolution palaeoenvironmental archive is the Lake Ohrid record located at 400 km to the SW of Harletz (Baumgarten et al., 2015; Sadori et al., 2016; Francke et al., 2016). In this reference record, MIS 7 corresponds to the upper part of palynozone OD-6 characterised by an alternation of coniferous and mesophylous forests with grassland (steppe) formations (Sadori et al., 2016); a vegetation which is in good accordance with the pedological signature of the basal soil complex at Harletz. The BFS complex developed in an alluvial plain environment from a parent material that is not loess, inducing a difference in soil facies with respect to contemporaneous S2 soil complexes occurring below L2 Late Saalian loess in regional records along the Danube from Serbia to the Romanian coast or to the Late Saalian loess of Western Europe (Fig. 10). In all the Danubian loess sections the S2 soil is described as a typical chernozem soil. In Harletz, the basal fluvial soil complex characteristics are more typical of a leached Cambisol indicating a riparian environment: more humid conditions and a forested landscape in accordance with its location within the Ogosta River alluvial plain, where trees or shrubs likely grew during MIS 7 (molluscs from forested environments), in contrast to slopes and plateaux covered by steppe vegetation, as today.

Overlying the Ogosta Soil Complex, the lower part of L2 loess includes an exceptionally detailed succession of loess and incipient soil horizons never described in European loess until now. The basal sequence of L2, denoted HZ-SL1, is very important as it testifies of a progressive step-by-step evolution of climate and of the environment during the transition between MIS 7 and MIS6 (Fig. 11). In Lake Ohrid reference pollen record, this transitional phase likely corresponds to palynozone OD5 between 190 and 160 ka (Sadori et al., 2016) characterised by a grassland-dominated environment (*Poaceae* and *Cyperaceae*). During this phase, a succession of 3–4 short (millennial) interstadial phases have been evidenced between 190 and 170 ka by both strong increases in mesophylous species (Sadori et al., 2016) and peaks in the TOC records (Francke et al., 2016). It is likely that they correspond to the succession represented by the soil of Unit 10 and incipient soils of Units 8, 6 and 4 in the Harletz loess record (Fig. 12). Global climate records, such as the deep-sea LR-04 global $\delta^{18}O$ records (Lisiecki and Raymo, 2005; Railsback et al., 2015), are not very contrasted over MIS 6. However, high-resolution $\delta^{18}O$ (*G. bulloides*) records from the Iberian margin (Hodell et al., 2013), provide evidence for a succession of short interstadial episodes spreading between about 190 and 165 ka that could be concomitant with the Harletz incipient soil horizons (Units 8, 6 and 4 in Fig. 12). The extremely cold and arid period of MIS 6 seems thus to last about 30 ka ($\approx$170–140 ka) in both Lake Ohrid, Harletz loess-palaeosol sequence, and Iberian margin marine records.

During the younger part of MIS6 (160-129ka), steppe vegetation with overwhelming herbs (*Artemisia*) is dominant (Sadori et al., 2016). This time interval (OD4 Zone) is characterised by the driest conditions observed in the 500 ka record of lake Ohrid and very similar vegetation history during this period is observed also in the pollen record from Tenaghi Phillipon in Greece (Tzedakis et al., 2003, 2006). This is in good accordance with a global enhancement of aeolian dynamics recorded in almost all the European loess section at that time (Fig. 10). It is especially the case in sections located close to the Danube River from Serbia to Bulgaria and Romania where L2 loess (MIS 6) always appears as the thickest loess interval of the entire loess-palaeosol record (Fig. 10). Even if during the last 200 ka, MIS 6 is considered as a very cold period it is not so different from MIS 2 in terms of ice volume and global climatic conditions, and the difference in aeolian sedimentary budgets could more likely result from a markedly longer period favourable to dust deflation during MIS 6 (ca. 35 ka) than during MIS 4 + 2 (ca. 25 ka).

The strong increase in loess sedimentation rates during MIS 6 is also recorded in Western Europe, for example, in Northern France (Antoine et al., 2015; Hérisson et al., 2016), Belgium (Juvigné et al., 1996; Vandenberghe et al., 1998; Meijs, 2002, 2011) or in Germany (Lehmkuhl et al., 2016). In Western Europe, late MIS 6 includes finely laminated loess facies with micro-frost cracks resulting from niveo-aeolian processes indicating a relatively important snow cover. This loess body is interrupted by up to five tundra gley horizons (15–20 cm thick) connected to large ice wedge casts networks (Meijs, 2000; Vandenberghe et al., 1998) testifying for ice-rich permafrost and markedly more humid conditions (snow cover) than in South-East Europe (Fig. 10).

However, even if the global context is very cold, lower aeolian dynamics and a sharp increase in biodiversity (molluscs) both characterise MIS 6 tundra gley horizons, as those from the Late Weichselian (Antoine et al., 2009a). This indicates that short (millennial) climatic oscillations had an impact on Western Europe during the lower half of the Late Saalian (Vandenberghe et al., 1998). Though these Western European Late Saalian loess sequences lack accurate age determinations, the similarity of their pedosedimentary succession with those from SE Europe loess allow to correlate tundra gley horizons of Western Europe to incipient soils at Harletz. This comparison seems to show that millennial climatic variability is recorded in aeolian sequences all over Europe, not only during the Last Glacial period, but also during the Penultimate glacial period. Finally, this episode characterised by high loess sedimentation rates in Europe corresponds to a global feature, which is contemporaneous of a strong maximum in dust concentrations in the EPICA Dome C record (Lambert et al., 2008).

At Harletz, the later stage of MIS 6 loess accumulation (subsequence HZ-SL3) shows a weakly weathered facies compared to the underlying pure sandy loess, indicating a progressive warming trend that is also well depicted in the Lake Ohrid record in the Upper part of OD-4 (138-128ka) during which the mesophylous species show a progressive increase to Interglacial values. This evolution seems to be characteristic of the upper part of L2 in the Lower Danube region suggesting that aeolian sedimentation strongly reduced but remained active during the transition to the Eemian and perhaps even during the interglacial itself. This contrasts with western European sections, where aeolian sedimentation clearly stops before the development of a down-building Interglacial brown leached soil, which overprints the previously decalcified loess.

4.3. Loess and sand sources, palaeo-wind implications

In the lower Danube area, during glacial times, the main source of silt and fine sands for loess deposition is the Danube braided alluvial plain. This is supported by observed variations in sequence thickness, average grain size, and distance from the Danube River (Jipa, 2014). Past wind directions have been reconstructed based on morphological constraints (Greda orientations: Rozycki, 1967) and grains size gradients relative to a Danubian source (Evlogiev, 2007; Jipa, 2014). Dominant wind directions are NW to W-NW in the middle and upper part of the Lower Danube, and N-NW to N directions when approaching the Black Sea (Fig. 1B). This pattern likely results from the deviation of the main winds by the Carpathian Mountains.

According to these interpretations, the silts and fine sands building the Harletz loess section would have been transported from the Danube braided river system located (at that time) about 4.5 km to the NW (Fig. 13A). The occurrence of high W-E to NW-SE elongated loess ridges (gredas), only on the right bank of the Ogosta River, is in accordance with the implied wind directions and indicate formation of gredas from Ogosta River sediments transported by west-northwest winds (Fig. 13A).

Based on our data, the main loess units, and especially Unit 3a, are characterised by a very low to a total absence of coarse sand particles (Fig. 5 and Table 2). According to the position of the section regarding the very close Ogosta alluvial plain, this observation implies that strong wind able to transport coarse sand grains (up to 2–3 mm) were not blowing from the East or Northeast during the Late Saalian. In addition, Saalian loess are characterised by a high proportion of fine sands (22–25% in the thick Unit 3a, Fig. 5). According to the absence of coarse particles originating from the Ogosta valley in Units 3a-3b, these fine sands (and coarse silts), which form the main component of Unit 3, were likely transported from Danube sources during northwestern storm events by saltation over about 4.5 km and over important topography separating the Danube Valley from the Harletz section (ca. 40 m in elevation at the base of the Harletz section, Fig. 13B). A similar case has been demonstrated for the Last Glacial in the Rhine River at Nussloch, where important amounts of fine sands deflated from the braided Rhine River have been transported (drifted) on the eastern slope and deposited on the plateau located at 3 km and 100 m above from the source by NW storms (Antoine et al., 2001).

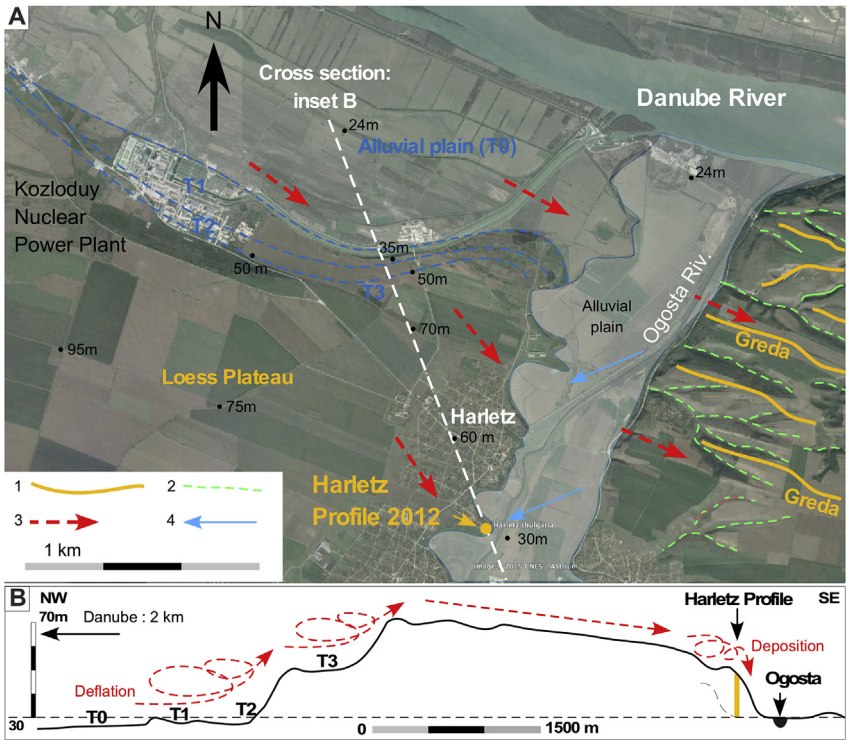

Fig. 13. A) Geomorphology of the Kozloduy-Harletz loess area, with location of the likely silt and sand sources area (alluvial plains) and palaeo-wind directions, location of the transect of Fig. 13B (topography according *Google Earth* Pro 2018*; Image © 2015 CNES/Astrium*). 1) Main loess gredas 2) dry valleys separating the gredas, 3) Main W-NW palaeo-wind direction, 4) Secondary E-NE palaeo-wind directions. **B)** NW-SE topographic cross section from the Danube alluvial plain to the Ogosta River at Harletz. Showing deflation area, transport distance and deposition zone (red dotted arrows). (For interpretation of the references to colour in this figure legend, the reader is referred to the Web version of this article.)

However, given the position of the studied section relative to the periglacial plain of the Ogosta River, one might expect that the Ogosta River alluvial plain was the major source of detrital material during glacial times. However, the analysis of sands sampled from the sandy-gravelly bottom of the current river shows that they are very rich in coarse sand grains and very fine gravels not observed in the loess of Unit 3. However, coarse sand percentages are the highest in the Harletz Soil Complex (Unit 2a-b, Fig. 5). As the percentage of coarse sands has been calculated independently of the other fractions (mass of grains > 160 μm/total mass of the sample), and also checked by the classical sieving method (Table 2 and red dots in Fig. 5), this result is not an artefact resulting from variations in the relative proportions of the fine and coarse sand components (Fig. 5). Taking into account this observation, it is clear that dominant wind regimes and thus climatic configurations have not been constant during the sedimentation of the Harletz sequence. It is therefore proposed that (Fig. 13):

1) during full glacial times, silts and fine sands accumulating to form the main loess units were transported from the braided river system of the Danube River during storm events blowing from W-NW. At that time, the topographic step between the steep slope of the left bank of the Ogosta valley and the alluvial plain produced a sediment trap allowing the downwind preservation of a thick loess sequence (Fig. 3). During full glacial times, the intensity of easterly-northeast winds is likely insufficient to transport coarse sand particles from the Ogosta River plain to the Harletz site.
2) During the Eemian interglacial, and to a lesser extent during interstadials, long distance transport of silt and fine sand particles characteristic of glacial periods is stopped but weak aeolian sedimentation is driven by north-easterly winds transporting coarse sand grains from the very proximal sandy banks of the Ogosta River on the ramp previously shaped during glacial loess deposition.
3) Lastly, the contrast between the thick Saalian accumulation and the thinner Last Glacial loess is likely linked to a change in topographical setting. The sediment trap favouring thick accumulation during the Saalian was rapidly filled during the Last Glacial enabling continued down wind transport. Since the Early Holocene, strong anthropogenic erosion in upper part of the sequence is also evidenced.

Finally, to interpret the absence of coarse sand grains in the whole Harletz loess deposits (especially during MIS6), without involving a change in wind directions, we could propose another hypothesis involving a change in the availability of coarse particles from the Ogosta River between glacial and interglacial times:

1) During glacial periods the development of a steppe in the Ogosta alluvial plain inhibits the transportation (saltation) of coarse particles to the valley slopes.
2) At the opposite, during interglacial periods the Ogosta River is characterised by a meandering system with large non vegetated sandy river banks exposed to deflation by NE winds and able to provide coarse sand grains during stormy events.

5. Conclusions

The multi-disciplinary approach and high-resolution investigations and luminescence dating undertaken on the 20 m thick Harletz loess-palaeosol section, coupled with a correlation

with other European loess and lacustrine reference records led to the following conclusions:

1) The lower 4 m of the profile are represented by an upbuilding brown soil complex (Ogosta Soil Complex) developed on alluvial silty sands deposited in the Ogosta River alluvial plain during an interglacial period that can be allocated to MIS 7.
2) The Harletz profile then exhibits a 10 m thick Late Saalian (MIS 6) loess accumulation that, until present, is remarkable in Europe.
3) The lower part of the main loess accumulation (HZ-SL1) includes an exceptionally thick (4 m) and detailed cyclic succession of four loess and four incipient soil horizons never described previously in European loess. This part of the record testifies of a progressive step-by-step evolution in the climate and in the environment during the transition from MIS 7 to MIS 6 and correlates well with the palynological record of Lake Ohrid (Sadori et al., 2016).
4) During the younger part of MIS 6 (160–129 ka), a global enhancement of the aeolian dynamics is evidenced during a period characterised by steppe vegetation with overwhelming herbs (*Artemisia*) in the Lake Ohrid record. This period is especially well recorded in sections located close to the Danube River from Serbia to Bulgaria and Romania (HZ-SL2/L2 loess).
5) The tephra occurring at 12 m depth within MIS 6 loess (HZ-SL2) represents an important element of comparison with sections in Romania and Serbia where a tephra was reported in the same stratigraphic position at the base of loess L2 at about 170–160 ka.
6) According to grain size and topographic data, silts and fine sands building the Harletz loess section during glacial periods would have been transported from the Danube braided river system located at that time at ca. 4.5 km to the NW. By contrast, during the Eemian interglacial, and to a lesser extent during MIS 5 and 3 interstadials, the long distance transport of silt and fine sand particles is stopped and a weak aeolian sedimentation is likely driven by north-easterly winds transporting coarse sand grains from the proximal sandy banks of the Ogosta River.
7) Finally, from a geomorphological point of view, this work provides geochronological constraints for the T2 terrace, allocating its formation to the cold stage directly preceding MIS 7 or MIS 8.

Data availability

The multi-proxy data sets presented in the present article will be made available on the Pangea data repository (https://www.pangaea.de/) once accepted.

Acknowledgments

This study benefited from research funds granted by the ANR to DDR (ACTES project ANR-08-BLAN-0227 - CSD 6), the CNRS-INSU SYSTER program to FL (2012-31124A) and the PHC Rila program to FL and DJ (34286QB). This is IPGP contribution n° 4006 and LDEO contribution 8271.

Appendix A. Supplementary data

Supplementary data to this article can be found online at https://doi.org/10.1016/j.quascirev.2019.01.005.

References

Almond, P.C., Tonkin, P.J., 1999. Pedogenesis by upbuilding in an extreme leaching and weathering environment, and slow loess accretion, south Westland, New Zealand. Geoderma 92, 1–36.
Antoine, P., Rousseau, D.-D., Zöller, L., Lang, A., Munaut, A.-V., Hatté, C., Fontugne, M., 2001. High-resolution record of the last interglacial-glacial cycle in the Nussloch loess-paleosol sequences, upper rhine area, Germany. Quat. Int. 76–77, 211–229.
Antoine, P., Rousseau, D.-D., Moine, O., Kunesch, S., Hatté, C., Lang, A., Tissoux, H., Zöller, L., 2009a. Rapid and cyclic aeolian deposition during the Last Glacial in European loess: a high-resolution record from Nussloch, Germany. Quat. Sci. Rev. 28, 2955–2973.
Antoine, P., Rousseau, D.D., Fuchs, M., Hatté, C., Marcovic, S.B., Jovanovic, M., Gaudenyi, T., Moine, O., Rossignol, J., 2009b. High resolution record of the last climatic cycle in the southern carpathian basin at Surduk (vojvodina, Serbia). Quat. Int. 198, 19–36.
Antoine, P., Rousseau, D.-D., Degeai, J.-P., Moine, O., Lagroix, F., Kreutzer, S., Fuchs, M., Hatté, C., Gauthier, A., Svoboda, J., Lisà, L., 2013. High-resolution record of the environmental response to climatic variations during the Last Interglacial–Glacial cycle in Central Europe: the loess-palaeosol sequence of Dolní Věstonice (Czech Republic). Quat. Sci. Rev. 67, 17–38.
Antoine, P., Limondin-Lozouet, N., Auguste, P., Locht, J.-L., Debenham, N., Bahain, J.-J., Goval, E., Fagnart, J.P., Ducrocq, T., 2015. Quaternary geoarchaeology and prehistory: the model of the Somme valley (France) and the neighbouring regions. In: Arnaud-Fassetta, G., Carcaud, N. (Eds.), French Geoarchaeology in the 21st Century. CNRS éditions, pp. 71–86.
Antoine, P., Coutard, S., Guérin, G., Deschodt, L., Goval, E., Locht, J.-L., Paris, C., 2016. Upper Pleistocene loess-palaeosols records from Northern France in the European context: environmental background and dating of the Middle Palaeolithic. Quat. Int. 411, 4–24.
Avramov, V.I., Jordanova, D., Hoffmann, V., Roesler, W., 2006. The role of dust source area and pedogenesis in three loess-palaeosol sections from North Bulgaria: a mineral magnetic study. In: Quaternary-International, Studia Geophysica et Geodaetica, 50. Springer, pp. 259–282.
Balescu, S., Lamothe, M., Panaiotu, C., Panaiotu, C., 2010. La chronologie IRSL des séquences loessiques de l'est de la Roumanie. Quaternaire 21 (2), 115–126.
Balsam, W.L., Ellwood, B.B., Ji, J.F., Williams, E.R., Long, X.Y., El Hassani, A., 2011. Magnetic susceptibility as a proxy for rainfall: worldwide data from tropical and temperate climate. Quat. Sci. Rev. 30 (19–20), 2732–2744.
Boch, R., Cheng, H., Spötl, C., Edwards, R.L., Wang, X., Häuselmann, P., 2011. NALPS: a precisely dated European climate record 120–60 ka. Clim. Past 7, 1247–1259.
Barker, S., Knorr, G., Edwards, L., Parrenin, F., Putnam, A.E., Skinner, L.C., Wolff, E., Ziegler, M., 2011. 800,000 Years of abrupt climate variability. Science 334, 347–351.
Baumgarten, H., Wonik, T., Tanner, D.C., Francke, A., Wagner, B., Zanchetta, G., Sulpizio, R., Giaccio,B, B., Nomade, S., 2015. Age-depth model of the past 630 kyr for Lake Ohrid (FYROM/Albania) based on cyclostratigraphic analysis of downhole gamma ray data. Biogeosciences 12, 7453–7465.
Cottereau, E., Arnold, M., Moreau, C., Baqué, D., Bavay, D., Caffy, I., Comby, C., Dumoulin, J.-P., Hain, S., Perron, M., Salomon, J., Setti, 2007. Artemis, the new 14C AMS at LMC14 in Saclay. France Radiocarbon 49, 291–299.
Dearing, J.A., Bird, P.M., Dann, R.J.L., Benjamin, S.F., 1997. Secondary ferrimagnetic minerals in Welsh soils: a comparison of mineral magnetic detection methods and implications for mineral formation. Geophys. J. Int. 130 (3), 727–736.
Debret, M., Sebag, D., Desmet, M., Balsam, W., Copard, Y., Mourier, B., Susperrigui, A.S., Arnaud, F., Bentaleb, I., Chapron, E., Lallier-Verges, E., Winiarski, T., 2011. Spectrocolorimetric interpretation of sedimentary dynamics: the new "Q7/4 diagram". Earth-Rev. Rev. 109, 1–19.
Desprat, S., Sánchez-Goñi, M.F., Naughton, F., Turon, J.-L., Duprat, J., Malaizé, B., Peypouquet, J.-P., 2007. Climate variability of the last five isotopic interglacials: direct land-sea-ice correlation from the multiproxy analysis of North-Western Iberian margin deep-sea cores. In: Sirocko, F., Claussen, M., Sánchez Goñi, M.F., Litt, T. (Eds.), The Climate of Past Interglacials. Elsevier, Amsterdam, pp. 375–386.
Eger, A., Almond, P.C., Condron, L.M., 2012. Upbuilding pedogenesis under active loess deposition in a super-humid, temperate climate-quantification of deposition rates, soil chemistry and pedogenic thresholds. Geoderma 189–190, 491–501.
Ehrmann, W., Schmiedl, G., Beuscher, S., Krüger, S., 2017. Intensity of african humid periods estimated from saharan dust fluxes. PLoS One 12 (1), e0170989. https://doi.org/10.1371/journal.pone.0170989.
Evlogiev, Y., 2007. Evidence for the aeolian origin of loess in the danubian plain. Geologica Balkanica 36 (3–4), 31–39.
Evlogiev, Y., 2015. In: Environment Impact Assessment Report on Investment Proposal "Construction of National Disposal Facility for Low and Intermediate Level Radioactive Waste – Ndf" - Part Iii, 2015, p. 98. Sofia.
Evstatiev, D., Angelova, R., Evlogiev, Y., 2000. Characteristics of loess as host media for radioactive waste disposal. In: 8th International IAEG Congress. Balkema, Rotterdam, pp. 4537–4544.
Eyre, J.K., 1997. Frequency dependence of magnetic susceptibility for populations of single-domain grains. Geophys. J. Int. 129, 209–211.
FAO UNESCO, 2014. World Soil Resources Report 106, World Reference Base for Soil Resources 2014 International Soil Classification System for Naming Soils and Creating Legends for Soil Maps, Update, p. 2015, 192p.
Francke, A., Wagner, B., Just, J., Leicher, N., Gromig, R., Baumgarten, H., Vogel, H., Lacey, J.H., Sadori, L., Wonik, T., Leng, M.J., Zanchetta, G., Sulpizio, R., Giaccio, B., 2016. Sedimentological processes and environmental variability at Lake Ohrid

(Macedonia, Albania) between 637 ka and the present. Biogeosciences 13, 1179–1196. https://doi.org/10.5194/bg-13-1179-2016, 2016.
Fuchs, M., Rousseau, D.D., Antoine, P., Hatté, C., Gauthier, C., 2007. Chronology of the last climatic cycle (upper pleistocene) of the Surduk loess sequence, vojvodina, Serbia. Boreas 10, 1–8.
Fuchs, M., Kreutzer, S., Rousseau, D.D., Antoine, P., Hatté, C., Lagroix, F., Moine, O., Gauthier, C., Svoboda, J., Lisá, L., 2013. The loess sequence of dolni vestonice (Czech republic): a new OSL based chronology of the last climatic cycle. Boreas 42, 664–677.
Fotakieva, E., Minkov, M., 1966. Der löß in bulgarien. Eiszeitalt. Ggw. 17, 87–96.
Gabris, G., 1994. Pleistocene evolution of the Danube in the carpathian basin. Terra. Nova 6, 495–501.
Gabris, G., Nador, A., 2007. Long-term fluvial archives in Hungary: response of the Danube and Tisza rivers to tectonic movements and climatic changes during the Quaternary: a review and new synthesis. Quat. Sci. Rev. 26 (22–24), 2758–2782.
Giosan, L., Coolen, M.J.L., Kaplan, J.O., Constantinescu, S., Filip, F., Filipova-Marinova, M., Kettner, A.J., Thom, N., 2012. Early anthropogenic transformation of the Danube-Black Sea system. Sci. Rep. 2, 582. https://doi.org/10.1038/srep00582.
Gauthier, C., Hatté, C., 2008. Effects of handling, storage, and chemical treatments on $\delta^{13}C$ values of terrestrial fossil organic matter. Geophysics, Geochemistry and Geosystem 9 (8). https://doi.org/10.1029/2008GC001967.
Gocke, M., Hambach, U., Eckmeier, E., Schwark, L., Zöller, L., Fuchs, M., Löscher, M., Wiesenberg, G.L.B., 2014. Introducing an improved multi-proxy approach for paleoenvironmental reconstruction of loess-paleosol archives applied on the Late Pleistocene Nussloch sequence (SW Germany). Palaeogeogr. Palaeoclimatol. Palaeoecol. 410, 300–315.
Haase, D., Fink, J., Haase, G., Ruske, R., Pécsi, M., Richter, H., Altermann, M., Jäger, K.-D., 2007. Loess in Europe - its spatial distribution based on a european loess map, 1:2 500 000. Quat. Sci. Rev. 26, 1301–1312.
Haesaerts, P., Metsdagh, H., 2000. Pedosedimentary evolution of the last interglacial and early glacial sequence in the European loess belt from Belgium to central Russia. Geol. Mijnb. 79 (2–3), 313–324.
Haesaerts, P., Borziak, I., Chirica, V., Damblon, F., Koulakovska, L., van der Plicht, J., 2003. the East carpathian loess record: a reference for the middle and late pleniglacial stratigraphy in central Europe. Quaternaire 14, 163–188.
Haesaerts, P., Damblon, F., Gerasimenko, N., Spagna, P., Pirson, S., 2016. The Late Pleistocene loess-palaeosol sequence of Middle Belgium. Quat. Int. 411, 25–43.
Hatté, C., Fontugne, M., Rousseau, D.-D., Antoine, P., Zöller, L., Tisnérat-Laborde, N., Bentaleb, I., 1998. $d^{13}C$ variations of loess organic matter as a record of the vegetation response to climatic changes during the Weichselian. Geology 26, 583–586.
Heiri, O., Koinig, K.A., Spötl, C., Barrett, S., Brauer, A., Drescher-Schneider, R., Gaar, D., Ivy-Ochs, S., Kerschner, H., Luetscher, M., Moran, A., Nicolussi, K., Preusser, F., Schmidt, R., Schoeneich, P., Schwörer, C., Sprafke, T., Terhorst, B., Tinner, W., 2014. Palaeoclimate records 60–8 ka in the Austrian and Swiss Alps and their forelands. Quat. Sci. Rev. 106, 186–205.
Hérisson, D., Coutard, S., Goval, E., Locht, J.-L., Antoine, P., Chantreau, Y., Debenham, N., 2016. A new key-site for the end of the lower palaeolithic and the onset of the middle palaeolithic at etricourt-manancourt (somme, France). Quat. Int. 409 (B), 73–91.
Hodell, D., Crowhurst, S., Skinner, L., Tzedakis, P.C., Margari, V., Channell, J.E.T., Kamenov, G., Maclachlan, S., Rothwell, G., 2013. Response of Iberian Margin sediments to orbital and suborbital forcing over the past 420 ka. Paleoceanography 28, 185–199. https://doi.org/10.1002/palo.20017.
Hošek, J., Hambach, U., Lisá, L., Matys Grygar, T., Horáček, I., Meszner, S., Knésl, I., 2015. An integrated rock-magnetic and geochemical approach to loess/paleosol sequences from Bohemia and Moravia (Czech Republic): implications for the Upper Pleistocene paleoenvironment in central Europe. Palaeogeogr. Palaeoclimatol. Palaeoecol. 418, 344–358.
Ji, J.F., Chen, J., Balsam, W., Lu, H.Y., Sun, Y.B., Xu, H.F., 2004. High resolution hematite/goethite records from Chinese loess sequences for the last glacial–interglacial cycle: rapid climatic response of the East Asian Monsoon to the tropical Pacific. Geophys. Res. Lett. 31.
Jipa, D.C., 2014. The loess-like deposits in the Lower Danube basin. Genetic significance. Geo-Eco-Marina 20, 7–18.
Jordanova, D., Petersen, N., 1999. Palaeoclimatic record from a loess-soil profile in northeastern Bulgaria. I. Rock magnetic properties. Geophys. J. Int. 138, 520–532.
Jordanova, D., Hus, J., Geeraerts, R., 2007. Palaeoclimatic implications of the magnetic record from loess/palaeosol sequence Viatovo (NE Bulgaria). Geophys. J. Int. 171, 1036–1047.
Jordanova, D., Hus, J., Evlogiev, J., Geeraerts, R., 2008. Palaeomagnetism of the loess/palaeosol sequence in Viatovo (NE Bulgaria) in the Danube basin. Phys. Earth Planet. In. 167, 71–83.
Juvigné, E., Haesaerts, P., Metsdagh, H., Balescu, S., 1996. Révision du stratotype loessique de Kesselt (Limbourg, Belgique). Compte Rendu de l'Académie des Sciences, Paris, série IIa 323, 801–807.
Konert, M., Vandenberghe, J., 1997. Comparison of laser grain size analysis with pipette and sieve analysis: a solution for the underestimation of the clay fraction. Sedimentology 44, 523–535.
Kukla, G., 1977. Pleistocene land-sea correlations. 1: Europe. Earth Sci. Rev. 13, 307–374.
Lambert, F., Delmonte, B., Petit, J.R., Bigler, M., Kaufmann, P.R., Hutterli, M.A., Stocker, T.F., Ruth, U., Steffensen, J.P., Maggi, V., 2008. Dust - climate couplings over the past 800,000 years from the EPICA Dome C ice core. Nature 452, 616–619. https://doi.org/10.1038/nature06763.
Lautridou, J.-P., Sommé, J., Heim, J., Puisségur, J.-J., et Rousseau, D.-D., 1985. La stratigraphie des loess et formations fluviatiles d'Achenheim (Alsace): nouvelles données bioclimatiques et corrélations avec les séquences pléistocènes de la France du Nord-Ouest. Bull. Assoc. Fr. Étude Quat. 22, 125–132.
Lehmkuhl, F., Zens, J., Krauß, L., Schulte, P., Kels, H., 2016. Loess-paleosol sequences at the northern European loess belt in Germany: distribution, geomorphology and stratigraphy. Quat. Sci. Rev. 153, 11–30.
Leicher, N., Zanchetta, G., Sulpizio, R., Giaccio, B., Wagner, B., Nomade, S., Francke, A., Del Carlo, P., 2016. First tephrostratigraphic results of the DEEP site record from Lake Ohrid (Macedonia and Albania). Biogeosciences 13, 2151–2178.
Li, B., Li, S.-H., 2011. Luminescence dating of K-feldspar from sediments: a protocol without anomalous fading correction. Quat. Geochronol. 6 (5), 468–479.
Lisiecki, L.E., Raymo, M.E., 2005. A Pliocene-Pleistocene stack of 57 globally distributed benthic $\delta^{18}O$ records. Paleoceanography 20, 1003. PA.
Luetscher, M., Boch, R., Sodemann, H., Spötl, C., Cheng, H., Edwards, R.L., Frisia, S., Hof, F., Müller, W., 2015. North atlantic storm track changes during the last glacial maximum recorded by alpine speleothems. Nat. Commun. 6, 1–6.
Lomax, J., Fuchs, M., Preusser, F., Fiebig, M., 2014a. Luminescence based loess chronostratigraphy of the Upper Palaeolithic site Krems-Wachtberg, Austria. Quat. Int. 351, 88–97.
Lomax, J., Kreutzer, S., Fuchs, M., 2014b. Performance tests using the Lexsyg luminescence reader. Geochronometria 41 (4).
Lomax, J., Fuchs, M., Antoine, P., Rousseau, D.-D., Lagroix, F., Hatté, D., Taylor, S., Till, J., Debret, M., Moine, O., Jordanova, D., January 2019. A luminescence-based chronology for the Harletz loess sequence, Bulgaria. Boreas 48 (1), 179–194. https://doi.org/10.1111/bor.12348.
Maher, B.A., Taylor, R.M., 1988. Formation of ultrafine-grained magnetite in soils. Nature 336, 368–371.
Margari, V., Skinner, L.C., Tzedakis, P.C., Ganopolski, A., Vautravers, M., Shackleton, N.J., 2010. The nature of millennial-scale climate variability during the past two glacial periods. Nat. Geosci. 3, 127–131.
Marković, S.B., Hambach, U., Catto, N., Jovanović, M., Buggle, B., Machalett, B., Zöller, L., Glaser, B., Frechen, M., 2009. The middle and late Pleistocene loess–paleosol sequences at Batajanica, Vojvodina, Serbia. Quat. Int. 198, 255–266.
Marković, S.B., Stevens, T., Kukla, G.J., Hambach, U., Fitzsimmons, K.E., Gibbard, P., Buggle, B., Zech, M., Guo, Z., Hau, Q., O'Hara, Dhand, K., Smalley, I., Újvári, G., Sümegi, P., Timar-Gabor, A., Veres, D., Sirocko, F., Jary, Z., Svensson, A., Jović, V., Kovács, J., Zvirčev, Z., Vasiljević, D.A., 2015. The Danube loess stratigraphy – new steps towards a pan-European loess stratigraphic model. Earth Sci. Rev. 148, 228–258.
Martrat, B., Grimalt, J.O., Lopez-Martinez, C., Cacho, I., Sierro, F.J., Flores, J.A., Zahn, R., Canals, M., Curtis, J.H., Hodell, D.A., 2004. Abrupt temperature changes in the western mediterranean over the past 250,000 years. Science 306, 1762–1765.
Martrat, B., Grimalt, J.O., Shackleton, N.J., de Abreu, L., Hutterli, M.A., Stocker, T.F., 2007. Four climate cycles of recurring deep and surface water destabilizations on the Iberian Margin. Science 317, 502–507.
Meijs, E.P.M., 2002. Loess stratigraphy in Dutch and Belgian limburg. Eiszeitalt. Ggw. 51, 114–130.
Meijs, E.P.M., 2011. The Veldwezelt site (province of Limburg, Belgium): environmental and stratigraphical interpretations. Netherlands Journal of Geosciences, Geologie en Mijnbouw 90, 73–94.
Moine, O., Rousseau, D.-D., Antoine, P., Hatté, C., 2002. Mise en évidence d'événements climatiques rapides par les faunes de mollusques terrestres des loess weichseliens de Nussloch (Allemagne). Quaternaire 13 (3–4), 209–218.
Moine, O., Rousseau, D.-D., Antoine, P., 2008. The impact of Dansgaard-Oeschger cycles on the loessic environment and malacofauna of Nussloch (Germany) during the Upper Weichselian. Quat. Res. 70, 91–104.
Moine, O., Antoine, P., Hatté, C., Landais, A., Mathieu, J., Prud'Homme, C., Rousseau, D.-D., 2017. The impact of Last Glacial climate variability in west-European loess revealed by radiocarbon dating of fossil earthworm granules. Proc. Acad. Nat. Sci. Philadelphia 24, 6209–6214. https://doi.org/10.1073/pnas.1614751114.
Mokeddem, Z., McManus, J.F., 2016. Persistent climatic and oceanographic oscillations in the subpolar North Atlantic during the MIS 6 glaciation and MIS 5 interglacial. Paleoceanography 31. https://doi.org/10.1002/2015PA002813.
Moreno, A., Svensson, A., Brooks, S.J., Connor, S., Engels, S., Fletcher, W., Genty, D., Heiri, O., Labuhn, I., Perşoiu, A., Peyron, O., Sadori, L., Valero-Garcés, B., Wulf, S., Zanchetta, G., contributors, d., 2014. A compilation of Western European terrestrial records 60–8 ka BP: towards an understanding of latitudinal climatic gradients. Quat. Sci. Rev. 106, 167–185.
Müller, U.C., Pross, J., Bibus, E., 2003. Vegetation response to rapid climate change in Central Europe during the past 140,000 yr based on evidence from the Füramoos pollen record. Quat. Res. 59, 235–245.
Murray, A., Wintle, A., 2000. Luminescence dating of quartz using an improved single-aliquot regenerative-dose protocol. Radiat. Meas. 32 (1), 57–73.
Murray, A., Wintle, A., 2003. The single aliquot regenerative dose protocol: potential for improvements in reliability. Radiat. Meas. 37 (4–5), 377–381.
Obreht, I., Zeeden, C., Hambach, U., Veres, D., Marković, S.B., Bösken, J., Svirčev, Z., Bačević, N., Gavrilov, M.B., Lehmkuhl, F., 2016. Tracing the influence of Mediterranean climate on Southeastern Europe during the past 350,000 years. Sci.

Rep. 6, 36334. https://doi.org/10.1038/srep36334.
Osipova, E., Danukalova, G., Markovic, S., 2013. Malacological characteristics of the Middle to Upper Pleistocene transitional interval (MIS 7-5) observed in the Batajnica locality (Serbia). Quat. Int. 292, 86–100.
Panaiotu, C.G., Panaiotu, E.C., Grama, A., Necula, C., 2001. Paleoclimatic record from a loessepaleosol profile in Southeastern Romania. Phys. Chem. Earth 26 (11–12), 893–898.
Railsback, L.B., Gibbard, P.L., Head, M.J., Voarintsoa, N.R.G., Toucanne, S., 2015. An optimized scheme of lettered marine isotope substages for the last 1.0 million years, and the climatostratigraphic nature of isotope stages and substages. Quat. Sci. Rev. 111, 94–106.
Radan, S.C., 2012. Towards a synopsis of dating the loess from the Romanian plain and Dobrogea: authors and methods through time. Geo-Eco-Marina 18, 153–172.
Rousseau, D.-D., Antoine, P., Hatté, C., Lang, A., Zöller, L., Fontugne, M., Ben Othman, D., Luck, J.-M., Moine, O., Labonne, M., Bentaleb, I., Jolly, D., 2002. Abrupt millennial climatic changes from Nussloch (Germany) upper weichselian eolian records during the last glaciation. Quat. Sci. Rev. 21, 1577–1582.
Rousseau, D.-D., Sima, A., Antoine, P., Hatté, C., Lang, A., Zöller, L., 2007. Link between European and North Atlantic abrupt climate changes over the last glaciation. Geophys. Res. Lett. 34 https://doi.org/10.1029/2007GL031716.
Rousseau, D.-D., Antoine, P., Gerasimenko, N., Sima, A., Fuchs, M., Hatté, C., Moine, O., Zöller, L., 2011. North Atlantic abrupt climatic events of the last glacial period recorded in Ukrainian loess deposits. Clim. Past 7, 221–234.
Rousseau, D.-D., Ghil, M., Kukla, G., Sima, A., Antoine, P., Fuchs, M., Hatté, C., Lagroix, F., Debret, M., 2013. Major dust events in Europe during during Marine isotope stage 5 (130-74 ka): a climatic interpretation of the “Markers”. Clim. Past 9, 2213–2230.
Rousseau, D.-D., Boers, N., Sima, A., Svensson, A., Bigler, M., Lagroix, F., Taylor, S., Antoine, P., 2017a. (MIS3 and 2) millennial oscillations in Greenland dust and Eurasian aeolian records – a paleosol perspective. Quat. Sci. Rev. 169, 99–113.
Rousseau, D.D., Svensson, A., Bigler, M., Sima, A., Steffensen, J.P., Boers, N., 2017b. Eurasian contribution to the last glacial dust cycle: how are loess sequences built? Clim. Past 13, 1181–1197.
Rozycki, St Zb, 1967. Le sens des verts portent la poussière de loess á la lumière de l'analyse des formes d'accumulation du loess en Bulgarie et en Europe Centrale. Rev. Geomorphol. Dyn. 1, 1–9.
Sadori, L., Koutsodendris, A., Panagiotopoulos, K., Masi, A., Bertini, A., Combourieu-Nebout, N., Francke, A., Kouli, K., Joannin, S., Mercuri, A.M., Peyron, O., Torri, P., Wagner, B., Zanchetta, G., Sinopoli, G., Donders, T.H., 2016. Pollen-based paleoenvironmental and paleoclimatic change at Lake Ohrid (south-eastern Europe) during the past 500 ka. Biogeosciences 13, 1423–1437.
Sánchez Goñi, M.F., Eynaud, F., Turon, J.-L., Shackleton, N.J., 1999. High resolution palynological record off the Iberian margin: direct land-sea correlation for the Last Interglacial complex. Earth Planet. Sci. Lett. 171, 123–137.
Sánchez Goñi, M.F., Cacho, I., Turon, J.-L., Guiot, J., Sierro, F.J., Peypouquet, J.-P., Grimalt, J., Shackleton, N.J., 2002. Synchroneity between marine and terrestrial responses to millenial scale climatic variability during the last glacial period in the mediterranean region. Clim. Dynam. 19, 95–105.
Sánchez Goñi, M.F., Landais, A., Fletcher, W.J., Naughton, F., Desprat, S., Duprat, J., 2008. Contrasting impacts of Dansgaard-Oeschger events over a western European latitudinal transect modulated by orbital parameters. Quat. Sci. Rev. 27, 1136–1151.
Schirmer, W., 2016. Late pleistocene loess of the lower rhine. Quat. Int. 411, 44–61.
Seelos, K., Sirocko, F., Dietrich, S., 2009. A continuous high-resolution dust record for the reconstruction of wind systems in central Europe (Eifel, Western Germany) over the past 133 ka. Geophys. Res. Lett. 36, 1–6.
Sirocko, F., Knapp, H., Dreher, F., Förster, M.W., Albert, J., Brunck, H., Veres, D., Dietrich, S., Zech, M., Hambach, U., Röhner, M., Rudert, S., Schwibus, K., Adams, C., und Sigl, P., 2016. The ELSA-Vegetation-Stack: reconstruction of Landscape Evolution Zones (LEZ) from laminated Eifel maar sediments of the last 60,000 years. Glob. Planet. Chang. 142, 108–135.
Stuiver, M., Polach, H.A., 1977. Discussion: reporting of ^{14}C data. Radiocarbon 19, 355–363.
Taylor, S.N., Lagroix, F., Rousseau, D.-D., Antoine, P., 2014. Mineral magnetic characterization of the Upper Pleniglacial Nussloch loess sequence (Germany): an insight into local environmental processes. Geophys. J. Int. 199 (3), 1463–1480.
Timar-Gabor, A., Wintle, A., 2013. On natural and laboratory generated dose response curves for 8 quartz of different grain sizes from Romanian loess. Quat. Geochronol. 18, 34–40.
Tisnérat-Laborde, N., Poupeau, J.-J., Tannau, J.-F., Paterne, M., 2001. Development of a semi-automated system for routine preparation of carbonate samples. Radiocarbon 43, 299–304.
Thompson, R., Maher, B.A., 1995. Age models, sediment fluxes and palaeoclimatic reconstructions for the Chinese loess and palaeosol sequences. Geophys. J. Int. 123, 611–622.
Tzedakis, P.C., Frogley, M.R., Heaton, T.H.E., 2003. Last Interglacial conditions in southern Europe: evidence from Ioannina, northwest Greece. Glob. Planet. Chang. 36, 157–170.
Tzedakis, P.C., Hooghiemstra, H., Pälike, H., 2006. The last 1.35 million years at Tenaghi Philippon: revised chronostratigraphy and long-term vegetation trends. Quat. Sci. Rev. 25, 3416–3430.
Újvári, G., Molnár, M., Novothny, A., Páll-Gergely, B., Kovács, J., Várhegyi, V., 2014. AMS ^{14}C and OSL/IRSL dating of the Dunaszekcső loess sequence (Hungary): chronology for 20 to 150 ka and implications for establishing reliable age–depth models for the last 40 ka. Quat. Sci. Rev. 106, 140–154.
Újvári, G., Stevens, T., Molnár, M., Demény, A., Lambert, Varga, G., Timothy Jull, A.J., Páll-Gergely, B., Buylaert, J.-P., Kovácsk, J., 2018. Coupled European and Greenland last glacial dust activity driven by North Atlantic climate. Proc. Natl. Acad. Sci. Unit. States Am. 114 (50), E10632–E10638. https://doi.org/10.1073/pnas.1712651114.
Varga, G., Kovács, J., Újvári, G., 2012. Late Pleistocene variations of the background aeolian dust concentration in the Carpathian Basin: an estimate using decomposition of grain-size distribution curves of loess deposits. Netherlands Journal of Geosciences, Geologie en Mijnbouw 91 (1/2), 159–171.
Varga, G., Cserhati, C., Kovacs, J., Szalai, Z., 2016. Saharan dust deposition in the Carpathian Basin and its possible effects on interglacial soil formation. Aeolian Research 22, 1–12.
Vandenberghe, J., Huijzer, A.S., Mücher, H., Laan, W., 1998. Short climatic oscillations in a western European loess sequence (Kesselt, Belgium). J. Quat. Sci. 13, 471–485.
Vandenberghe, J., 2013. Grain size of fine-grained windblown sediment: a powerful proxy for process identification. Earth Sci. Rev. 121, 18–30.
Yang, S., Ding, Z., 2014. A 249 kyr stack of eight loess grain size records from northern China documenting millennial-scale climate variability. Geochemistry, Geophysics, Geosystems 15 (3), 789–814.
Zhou, L.-P., Oldfield, F., Wintle, A.G., Robinson, S.G., Wang, J.T., 1990. Partly pedogenic origin of magnetic variations in Chinese loess. Nature 346, 737–739.